Dynamics and thermalization of the nuclear spin bath in the single-molecule magnet Mn_{12}-ac: Test for the theory of spin tunneling

Andrea Morello*
Kamerlingh Onnes Laboratory, Leiden University, P.O. Box 9504, 2300RA Leiden, The Netherlands;
Department of Physics and Astronomy, University of British Columbia, Vancouver, British Columbia, Canada V6T 1Z1;
and ARC Centre of Excellence for Quantum Computer Technology, School of Electrical Engineering and Telecommunications, The University of New South Wales, Sydney NSW 2052, Australia

L. J. de Jongh
Kamerlingh Onnes Laboratory, Leiden University, P.O. Box 9504, 2300RA Leiden, The Netherlands
(Received 19 June 2007; revised manuscript received 17 October 2007; published 20 November 2007)

The description of the tunneling of a macroscopic variable in the presence of a bath of localized spins is a subject of great fundamental and practical interest, and is relevant for many solid-state qubit designs. Most of the attention is usually given to the dynamics of the "central spin" (i.e., the qubit), while little is known about the spin bath itself. Here, we present a detailed study of the dynamics of the nuclear spin bath in the Mn_{12}-ac single-molecule magnet, probed by NMR experiments down to very low temperatures ($T \simeq 20$ mK). The results are critically analyzed in the framework of the Prokof'ev-Stamp theory of nuclear-spin-mediated quantum tunneling. We find that the longitudinal relaxation rate of the ^{55}Mn nuclei in Mn_{12}-ac becomes roughly T independent below $T \simeq 0.8$ K and can be strongly suppressed with a longitudinal magnetic field. This is consistent with the nuclear relaxation being caused by quantum tunneling of the molecular spin, and we attribute the tunneling fluctuations to the minority of fast-relaxing molecules present in the sample. The transverse nuclear relaxation is also T independent for $T < 0.8$ K, and can be explained qualitatively and quantitatively by the dipolar coupling between like nuclei in neighboring molecules. This intercluster nuclear spin diffusion mechanism is an essential ingredient for the global relaxation of the nuclear spin bath. We also show that the isotopic substitution of ^{1}H by ^{2}H leads to a slower nuclear longitudinal relaxation, consistent with the decreased tunneling probability of the molecular spin. Finally, we demonstrate that even at the lowest temperatures—where only T-independent quantum tunneling fluctuations are present—the nuclear spins remain in thermal equilibrium with the lattice phonons, and we investigate the time scale for their thermal equilibration. After a review of the theory of macroscopic spin tunneling in the presence of a spin bath, we argue that most of our experimental results are consistent with that theory, but the thermalization of the nuclear spins is not. This calls for an extension of the spin-bath theory to include the effect of spin-phonon couplings in the nuclear-spin-mediated tunneling process.

DOI: 10.1103/PhysRevB.76.184425 PACS number(s): 75.45.+j, 76.60.−k, 03.65.Yz

I. INTRODUCTION

The understanding of quantum tunneling in mesoscopic systems has made a huge progress in the past decades to the point that nanofabricated devices are now being exploited as coherently tunneling two-level systems (TLSs) for quantum information purposes.[1–3] Conceptually, a first breakthrough was the proper description of the coupling of an effective TLS to an environment described by an oscillator bath.[4] Whether the system is an intrinsic TLS (e.g., a spin $s=1/2$) or the low-energy truncation of a more complicated entity (e.g., the flux state of a superconducting quantum interference device), one can generally apply the oscillator bath theory when the environment is described by delocalized modes (conduction electrons, phonons, photons, etc.), and the couplings of the TLS to each oscillator are weak. In many solid-state systems, however, it can be necessary to account for localized environmental excitations whose couplings to the TLS are not weak. This type of environment is called "spin bath"[5–7] and cannot be mapped onto an oscillator bath. Importantly, a spin-bath environment can cause decoherence even at $T=0$ and is therefore of great relevance for quantum systems that are designed to show coherent dynamics, like qubits for quantum computation. The prototypical realization of a tunneling TLS coupled to a spin bath is the giant spin of a single-molecule magnet (SMM).[8–10] These molecular systems consist of a core of strongly interacting transition metal ions, surrounded by organic ligands. At sufficiently low temperatures, the core of the molecule behaves effectively like a single large spin **S**. When uniaxial magnetic anisotropy is present, the reversal of the spin direction requires—classically—a large energy, so that the spin direction can be frozen at very low T. However, in the presence of a transverse magnetic field or a biaxial anisotropy, the spin direction can be reversed by tunneling through the anisotropy barrier.[11] The electronic spins that form the SMM are magnetically coupled to the nuclear spins that either belong to the magnetic ions themselves (^{55}Mn, ^{56}Fe,…) or to the surrounding ligand molecules (^{1}H, ^{13}C,…). As a consequence of these couplings, the observation of macroscopic quantum tunneling of magnetization in SMMs[10,12–15] cannot be understood without invoking the dynamics of the nuclear spins themselves.[6] The theoretical predictions for the role of nuclear spins in the magnetization tunneling of SMMs[16] have

been verified by a series of experiments on the Fe_8 compound.[17,18] Most remarkably, this material allows us to change the isotopic composition of the sample, both by strengthening ($^{56}Fe \rightarrow {}^{57}Fe$ substitution) and weakening ($^{1}H \rightarrow {}^{2}H$ substitution) the hyperfine couplings while leaving the electronic structure of the SMMs unaffected. As predicted, the rate of quantum relaxation of the magnetization was found to be directly related to the nuclear isotopic composition of the sample.[18] More recently, the effect of isotopic substitution has been observed in the low-T electronic specific heat of Fe_8 (Ref. 19) and in the dephasing time of coherent electron spin precession in Cr_7Ni.[20] Nuclear spin effects were also invoked in the interpretation of muon spin resonance data in isotropic molecules[21] and in an alternative description of the short-term magnetic relaxation in SMMs.[22] All these works have analyzed the effect of the nuclei on the dynamics of the "central spin," but a crucial aspect of the theory of the spin bath is that the tunneling of the central system has repercussion on the dynamics of the bath itself, so that the latter cannot be simply regarded as an independent source of "noise." Until now, the experiments to probe the electron spin dynamics have not been able to test this delicate aspect of the theory. To understand the details of the nuclear spin fluctuations, one should then look *directly* at the nuclear spins by means of low-temperature NMR experiments, performed under different regimes for the quantum dynamics of the electron spin. These experiments have been carried out by several groups,[23–27] but an accurate analysis of their implications for the more general theory of nuclear-spin mediated quantum tunneling is still lacking.

In this work, we present a comprehensive set of experiments on the dynamics of ^{55}Mn nuclear spins in the Mn_{12}-ac SMM, and we use our results for a critical assessment of the theory of the spin bath. Our data provide definitive proof that the nuclear spin dynamics is strongly correlated with that of the central spin; that is, it cannot be treated as an independent source of noise. Indeed, we find that the nuclear spin fluctuations change dramatically when the tunneling dynamics of the central spin is modified, e.g., by an external magnetic field. In addition, we shall demonstrate that the nuclear spins remain in thermal equilibrium with the phonon bath down to the lowest temperatures ($T \simeq 20$ mK) accessible to our experiment, where the thermal fluctuations of the electron spins are entirely frozen out. This implies that there is a mechanism for exchanging energy between nuclei, electrons, and phonons *through the nuclear-spin-mediated quantum tunneling of the central spin*. This is the point where the current theoretical description of macroscopic quantum tunneling in the presence of a spin bath needs to be improved.

As regards the "macroscopicness" of the quantum effects observed in SMMs, we adopt Leggett's view that the most stringent criterion is the "disconnectivity,"[28,29] $\mathcal{D}$, which, roughly speaking, is the number of particles that behave differently in the two branches of a quantum superposition. For instance, while a Cooper pair box[1] is a relatively large, lithographically fabricated device, the quantum superposition of its charge states involves, in fact, only one Cooper pair, i.e., two electrons, and its disconnectivity is only $\mathcal{D}=2$. The matter-wave interference in fullerene molecules,[30] for instance, is a much more "quantum macroscopic" phenomenon since it means that $60\times(12 \text{ nucleons}+6 \text{ electrons})=1080$ particles are superimposed between different paths through a diffraction grating. For the spin tunneling in Mn_{12}-ac SMMs discussed here, we have 44 electron spins simultaneously tunneling between opposite directions, which places this system logarithmically halfway between single particles and fullerenes on a macroscopicness scale.

The paper is organized as follows. Section II describes the physical properties of the sample used in the experiments, the design and performance of our measurement apparatus, and the methods of data analysis. Section III presents the experimental results on the nuclear spin dynamics, starting with the NMR spectra, the longitudinal and transverse relaxation rates in zero field, and their dependence on a longitudinal external field. We also study the nuclear relaxation in different Mn sites within the cluster and the effect of isotopic substitution in the ligand molecules. In Sec. IV, we discuss the thermal equilibrium between nuclear spins and phonon bath, the experimental challenges in optimizing it, and the indirect observation of magnetic avalanches during field sweeps. In Sec. V, we give an introductory review of the theory of the spin bath and apply its predictions to the calculation of the nuclear relaxation rate as observed in our experiments. Together with the information on the thermal equilibrium of the nuclear spins, this will allow us to draw clear-cut conclusions on the status of our current theoretical understanding of quantum tunneling of magnetization. We conclude with a summary and implications of the results in Sec. VI.

II. EXPERIMENT

A. Sample properties

We chose to focus our study on the well-known $[Mn_{12}O_{12}(O_2CMe)_{16}(H_2O)_4]$ (Mn_{12}-ac) compound, which belongs to the family of SMMs with the highest anisotropy barrier. As we shall see below, the rationale for choosing a SMM with high anisotropy barrier is that the electron spin fluctuations become slow on the NMR time scale at temperatures of a few kelvins. The structure of the cluster[31] (Fig. 1) consists of a core of four Mn^{4+} ions with electron spin $s=3/2$, which we shall denote as $Mn^{(1)}$, and eight Mn^{3+} ions ($s=2$) on two inequivalent crystallographic sites, $Mn^{(2)}$ and $Mn^{(3)}$ [Fig. 1(a)]. Within the molecular cluster, the electron spins are coupled by mutual superexchange interactions, the strongest being the antiferromagnetic interaction between $Mn^{(1)}$ and $Mn^{(2)}$ (Ref. 32). The molecules crystallize in a tetragonal structure with lattice parameters $a=b=17.319$ Å and $c=12.388$ Å. The ground state of the molecule has a total electron spin $S=10$ and, for the temperature range of interest in the present work ($T<2$ K), we may describe the electron spin of the cluster by means of the effective spin Hamiltonian

$$\mathcal{H} = -DS_z^2 - BS_z^4 + E(S_x^2 - S_y^2) - C(S_+^4 + S_-^4) + \mu_B \mathbf{B}\cdot\mathbf{g}\cdot\mathbf{S}. \quad (1)$$

Commonly adopted parameter values are $D=0.548$ K, $B=1.17$ mK, and $C=22$ μK, as obtained by neutron scattering

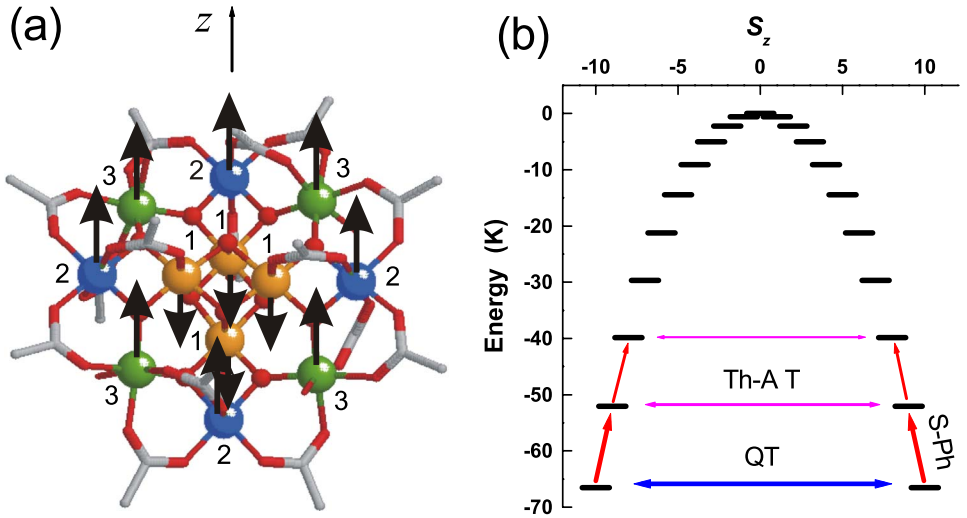

FIG. 1. (Color online) (a) Structure of the Mn_{12}-ac cluster, with the labeling of the three inequivalent Mn sites as described in the text. (b) Energy level scheme for the electron spin as obtained from the Hamiltonian [Eq. (1)], retaining only the terms diagonal in S_z. The nondiagonal terms allow transitions between states on opposite sides of the anisotropy barrier by means of quantum tunneling (QT). In the presence of intrawell transitions induced by spin-phonon interaction (S-Ph), thermally assisted quantum tunneling (Th-A T) between excited doublets can also take place.

data,[33] and for the **g** tensor the values $g_{\parallel}=1.93$ and $g_{\perp}=1.96$ from high-frequency EPR.[34–36] The uniaxial anisotropy terms $-DS_z^2$ and $-BS_z^4$ can be attributed to the single-ion anisotropy of the Mn^{3+} ions,[34] which is due to the crystal field effects resulting in the Jahn-Teller distortions of the coordination octahedra, where the elongation axes are approximately parallel to the $\hat{c}$ axis of the crystal. Considering only the diagonal terms, the energy level scheme would be a series of doublets of degenerate states, $|\pm m\rangle$, separated by a barrier with a total height of $DS^2+BS^4\simeq 66.6$K [Fig. 1(b)]. The transverse anisotropy terms, $E(S_x^2-S_y^2)-C(S_+^4+S_-^4)$, lift the degeneracy of the $|\pm m\rangle$ states and allow quantum tunneling of the giant spin through the anisotropy barrier. We call Δ_m the matrix element for the tunneling of the giant spin through the mth doublet, and $2\Delta_m$ the corresponding tunneling splitting. The $C(S_+^4+S_-^4)$ term arises from the fourfold S_4 point symmetry of the molecule, but there is now solid experimental evidence[37,38] for the prediction[39] that a disorder in the acetic acid of crystallization is present and gives rise to six different isomers of Mn_{12} cluster, four of which have symmetry lower than tetragonal and therefore have a nonzero rhombic term $E(S_x^2-S_y^2)$. EPR experiments give an upper bound $E\leqslant 14$ mK.[37] For the purpose of NMR experiments, such isomerism may cause slight variations in the local hyperfine couplings, causing extra broadening in the ^{55}Mn resonance lines. Very recently, a new family of Mn_{12} clusters has been synthesized, which does not suffer from the solvent disorder mentioned above and yields indeed more sharply defined ^{55}Mn NMR spectra.[40]

When adding spin-phonon interactions,[41,42] the possible transitions between the energy levels of Eq. (1) are sketched in Fig. 1(b). We distinguish between *intrawell* spin-phonon excitations, where the spin state remains inside the same energy potential well, and the *interwell* transitions, which involve spin reversal by quantum tunneling through the barrier, allowed by the terms in Eq. (1) that do not commute with S_z. Thermally assisted tunneling involves both these types of transitions.

The above discussion refers to the majority of the molecules in a real sample, but for our experiments, the crucial feature of Mn_{12}-ac is the presence of fast-relaxing molecules (FRMs),[43] i.e., clusters characterized by a lower anisotropy barrier and a much faster relaxation rate, as observed for instance by *ac* susceptibility[44] and magnetization measurements.[45] It has been recognized that such FRMs originate from Jahn-Teller isomerism,[46] i.e., the presence in the molecule of one or two Mn^{3+} sites where the elongated Jahn-Teller axis points in a direction roughly perpendicular instead of parallel to the crystalline $\hat{c}$ axis. This results in the reduction of the anisotropy barrier to 35 or 15 K in the case of one or two flipped Jahn-Teller axes, respectively,[47] and presumably in an increased strength of the nondiagonal terms in the spin Hamiltonian as well. Furthermore, the anisotropy axis z of the whole molecule no longer coincides with the crystallographic $\hat{c}$ axis, but deviates, e.g., by $\sim 10°$ in the molecules with a 35 K barrier.[45] The Jahn-Teller isomerism is very different from the above-mentioned effect of disorder in solvent molecules and produces much more important effects for the present study. As will be argued below, the presence of the FRMs is essential for the interpretation of our results and, to some extent, may be regarded as a fortunate feature for this specific experiment.

The sample used in the experiment consisted of about 60 mg of polycrystalline Mn_{12}-ac, with a typical crystallite volume ~ 0.1 mm^3. The crystallites were used as grown (i.e., not crushed), mixed with Stycast 1266 epoxy, inserted in a ⌀ 6 mm capsule, and allowed to set for 24 h in the room-temperature bore of a 9.4 T superconducting magnet. With this procedure, the magnetic easy axis of the molecules (which coincides with the long axis of the needlelike crystallites) ends up being aligned along the field within a few

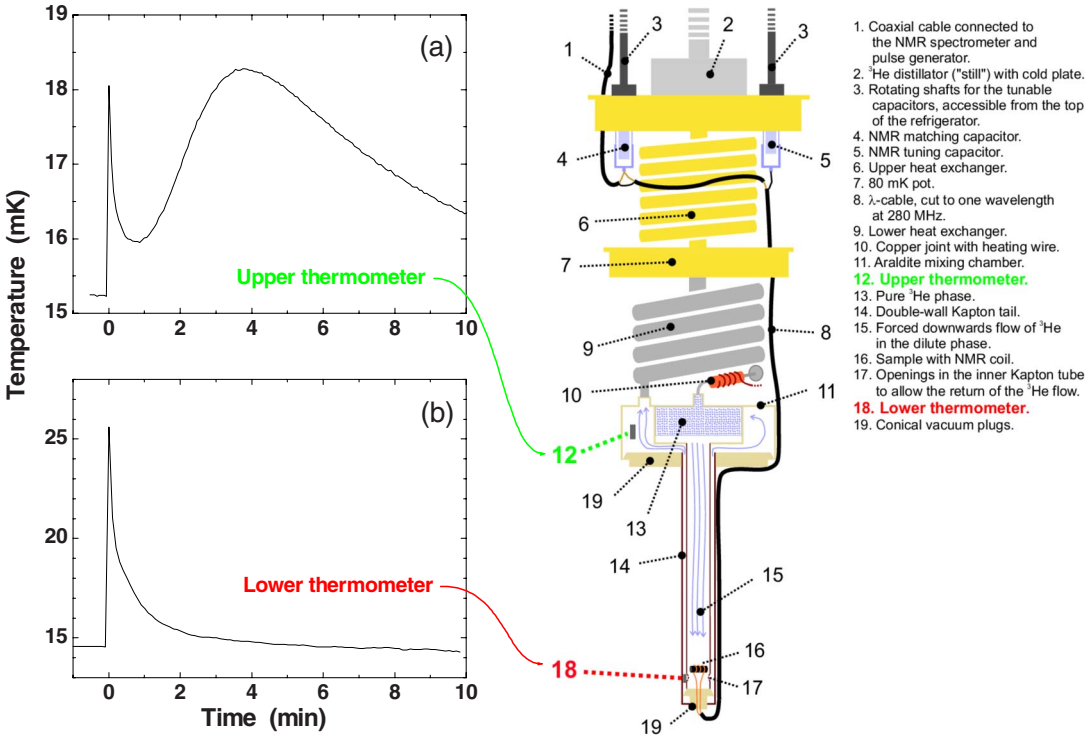

FIG. 2. (Color online) Sketch of the low-temperature part of the dilution refrigerator, showing the components of the NMR circuitry, the special plastic mixing chamber, and the position of the thermometers. Graph panels: temperatures recorded at the (a) upper and (b) lower mixing chamber thermometers, having applied a spin-echo NMR pulse sequence at time $t=0$.

degrees. In addition, we shall report NMR spectra taken on a small single crystal (mass $\sim$1 mg).

B. Low-temperature pulse NMR setup

Our experimental setup is based on a Leiden Cryogenics MNK126-400ROF dilution refrigerator, fitted with a plastic mixing chamber that allows the sample to be thermalized directly by the ^{3}He flow. A scheme of the low-temperature part of the refrigerator is shown in Fig. 2, together with the NMR circuitry. The mixing chamber consists of two concentric tubes, obtained by rolling a Kapton foil coated with Stycast 1266 epoxy. The tops of each tube are glued into concentric Araldite pots: The inner pot receives the downward flow of condensed ^{3}He and, a few millimeters below the inlet, the phase separation between the pure ^{3}He phase and the dilute ^{3}He/^{4}He phase takes place. The circulation of ^{3}He is then forced downward along the inner Kapton tube, which has openings at the bottom side to allow the return of the ^{3}He stream through the thin space in between the tubes. Both the bottom of the Kapton tail and the outer pot are closed by conical Araldite plugs smeared with Apiezon N grease.

A two-turn copper coil is wound around the capsule containing the sample, mounted on top of the lower conical plug and inserted in the ^{3}He/^{4}He mixture at the bottom of the mixing chamber tail, which coincides with the center of a 9 T superconducting magnet. The coil is then connected by a thin brass coaxial cable (length $\approx$0.5 m) to two tunable cylindrical Teflon capacitors, mounted at the still (see Fig. 2). At the frequency where the cable connecting capacitors and coil is precisely one wavelength, the circuit is equivalent to a standard lumped LC resonator. However, since the λ cable is a low-conductivity coax for low-T applications, the quality factor of the resonator (which includes the cable) is drastically reduced. Although this affects the sensitivity of the circuit, it also broadens the accessible frequency range without the need to retune the capacitors. Cutting the cable for one wavelength at $\sim$280 MHz, the circuit is usable between (at least) 220 and 320 MHz. As for the room-temperature NMR electronics, details can be found in Ref. 48.

The temperature inside the mixing chamber is monitored by two simultaneously calibrated Speer carbon thermometers, one in the outer top Araldite pot and the other at the bottom of the Kapton tail, next to the sample. At steady state and in the absence of NMR pulses, the temperature along the mixing chamber is uniform within $\lesssim$0.5 mK. The effect of applying high-power ($\sim$100 W) NMR pulses is shown in Figs. 2(a) and 2(b). A sudden increase in the measured temperature is seen both at the bottom and the top thermometer, and can be attributed to the short electromagnetic pulse. The temperature at the lower thermometer, i.e., next to the sample and the NMR coil, quickly recovers its unperturbed value, whereas the upper thermometer begins to sense the "heat wave" carried by the ^{3}He stream with a delay of about 3 min. This has the important consequence that we can use the upper thermometer to distinguish the effect of sudden electromagnetic radiation bursts from the simple heating of the ^{3}He/^{4}He mixture, as will be shown in Sec. IV B below.

The sample temperature is regulated by applying current to a Manganin wire, anti-inductively wound around a copper

joint just above the ^{3}He inlet in the mixing chamber. In this way, we can heat the incoming ^{3}He stream and uniformly increase the mixing chamber temperature.

For the ^{3}He circulation, we employ an oil-free pumping system, consisting of a 500 m^3/h root booster pump, backed by two 10 m^3/h dry scroll pumps. The system reaches a base temperature of 9 mK, and the practical operating temperature while applying rf pulses is as low as 15–20 mK.

C. Measurements and data analysis

The ^{55}Mn nuclear precession was detected by the spin-echo technique. A typical pulse sequence includes a first $\pi/2$ pulse with a duration of $t_{\pi/2}=12$ μs, a waiting interval of 45 μs, and a 24 μs π pulse for refocusing. Given the heating effects shown in Fig. 2, a waiting time of 600 s between subsequent pulse trains easily allows us to keep the operating temperature at around 15–20 mK. Moreover, at such low temperature, the signal intensity is so high that we could obtain an excellent signal-to-noise ratio without the need of averaging, so that a typical measurement sequence took less than 12 h. Above 100 mK, it proved convenient to take a few averages, but there the heating due to the rf pulses became negligible, and the waiting time could be reduced to ~100 s.

The longitudinal spin relaxation (LSR) was studied by measuring the recovery of the longitudinal nuclear magnetization after an inversion pulse. We preferred this technique to the more widely used saturation recovery[24,49,50] because it avoids the heating effects of the saturation pulse train, but we checked at intermediate temperatures that the two methods indeed lead to the same value of LSR rate. An example of echo signals obtained as a function of the waiting time after the inversion pulse is shown in Fig. 3(a). By integrating the echo intensity, we obtain the time dependence of the nuclear magnetization, $M(t)$, as shown in Fig. 3(b). For ease of comparison between different curves, we renormalize the vertical scale such that $M(0)/M(\infty)=-1$ and $M(t\gg T_1)/M(\infty)=1$, even though usually $|M(0)|<|M(\infty)|$, as could be deduced from Fig. 3(a). This is just an artifact that occurs when the NMR line is much broader than the spectrum of the inversion pulse, and does not mean that the length of the π pulse is incorrect. Since the ^{55}Mn nuclei have spin $I=5/2$, we fitted the recovery of the nuclear magnetization with[51]

$$\frac{M(t)}{M(\infty)} = 1 - \left[\frac{100}{63}e^{-30Wt} + \frac{16}{45}e^{-12Wt} + \frac{2}{35}e^{-2Wt}\right], \quad (2)$$

where W is the longitudinal spin relaxation rate. Note that in the simple case of a spin 1/2, W is related to the relaxation time T_1 by $2W=T_1^{-1}$. The above multiexponential expression and its numerical coefficients are derived under the assumption that the $I=5/2$ multiplet is split by quadrupolar interactions, and it is possible to resolve the central transition within that multiplet. While earlier work indicated that all three manganese NMR lines are quadrupolar split,[50] more recent experiments on single-crystal samples have questioned that conclusion[27,40] and, thereby, the applicability of Eq. (2) to the present experiments. Even if other sources of line broadening hinder the visibility of the quadrupolar contribution, the condition for the absence of quadrupolar splitting is an exactly cubic environment for the nuclear site, which is not satisfied here. For this reason and for ease of comparison with our[23,52] and other groups' earlier results,[24,49,50] we choose to retain Eq. (2) for the analysis of the inversion recovery data.

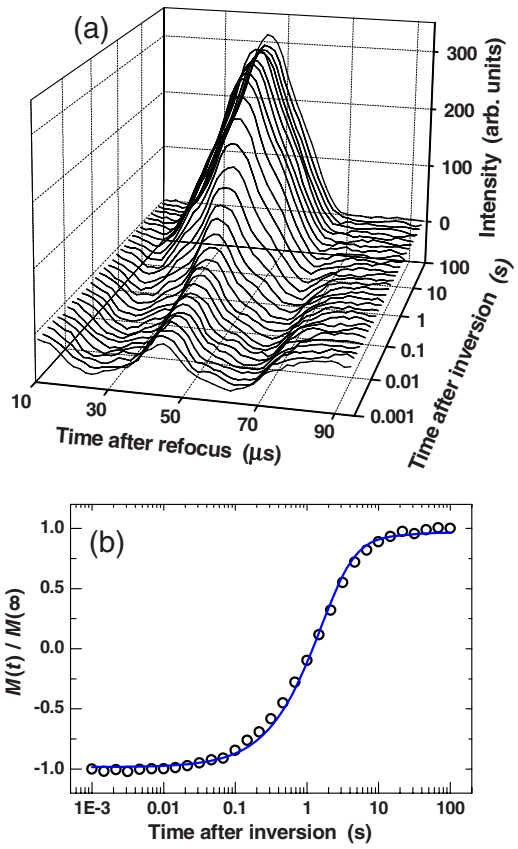

FIG. 3. (Color online) (a) An example of "real time" echo signals recorded during an inversion recovery, i.e., measuring the echo intensity at increasing delays after an inversion pulse. In particular, these are single-shot (no averaging) raw data taken at $B=0$ and $T=20$ mK in the $Mn^{(1)}$ site. (b) The (normalized) integral of the echoes (open dots) is fitted to Eq. (2) (solid line) to yield the LSR rate W.

The transverse spin relaxation (TSR) rate T_2^{-1} was obtained by measuring the decay of echo intensity upon increasing the waiting time τ between the $\pi/2$ and the π pulses. The decay of transverse magnetization $M_\perp(\tau)$ can be fitted by a single exponential

$$\frac{M_\perp(2\tau)}{M_\perp(0)} = \exp\left(-\frac{2\tau}{T_2}\right), \quad (3)$$

except at the lowest temperatures ($T\lesssim 0.2$ K), where also a Gaussian component T_{2G}^{-1} needs to be included,

$$\frac{M_\perp(2\tau)}{M_\perp(0)} = \exp\left(-\frac{2\tau}{T_2}\right)\exp\left(-\frac{(2\tau)^2}{2T_{2G}^2}\right). \quad (4)$$

As regards the experiments to determine the nuclear spin temperature, the measurements were performed by monitoring the echo intensity at regular intervals while changing the

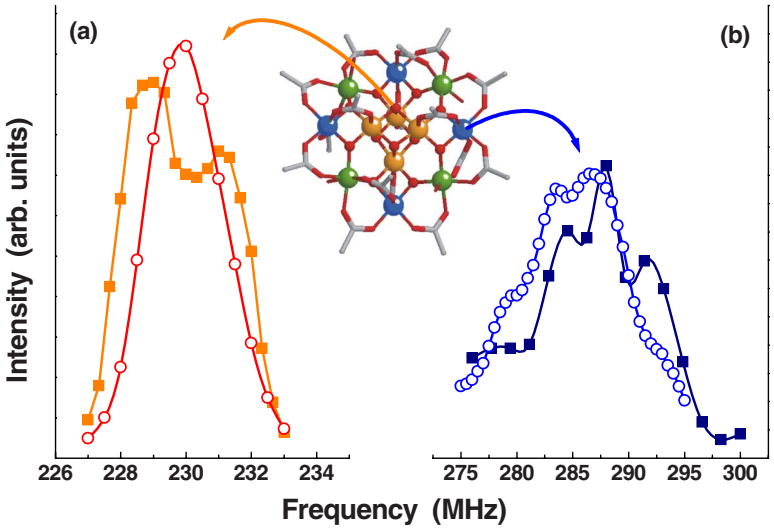

FIG. 4. (Color online) ^{55}Mn NMR spectra of the (a) $Mn^{(1)}$ and (b) $Mn^{(2)}$ lines in Mn_{12}-ac at $T=20$ mK. Open circles: oriented powder. Solid squares: single crystal. The Mn sites corresponding to each line are shown in the central drawing of the molecular structure. All the spectra are measured in a field-cooled sample.

temperature T_{bath} of the ^{3}He/^{4}He bath in which the sample is immersed. Recalling that the nuclear magnetization is related to the nuclear spin temperature T_{nucl} by the Curie law,

$$M(T_{\text{nucl}}) = N\mu_0 \frac{\hbar^2 \gamma_N^2 I(I+1)}{3k_B T_{\text{nucl}}}, \tag{5}$$

and assuming that $T_{\text{bath}}=T_{\text{nucl}}$ at a certain temperature T_0 (e.g., 0.8 K), we can define a calibration factor K such that $M(T_0)=K/T_{\text{nucl}}(T_0)$ and use that definition to derive the time evolution of the nuclear spin temperature as $T_{\text{nucl}}(t)=K/M(t)$ while the bath temperature is changed.

Due to the strong magnetic hysteresis of Mn_{12}-ac, it is important to specify the magnetization state of the sample since, as will be shown below, this parameter can influence the observed nuclear spin dynamics. Therefore, we carried out experiments under both zero-field cooled (ZFC) and field-cooled (FC) conditions, which correspond to zero and saturated magnetization along the easy axis, respectively. Heating the sample up to $T\approx 4$ K is sufficient to wash out any memory of the previous magnetic state. When the sample is at $T\ll 1$ K, the field-cooling procedure can be replaced by the application of a longitudinal field large enough to destroy the anisotropy barrier, e.g., $B_z=8$ T. Importantly, the shift of the ^{55}Mn NMR frequency with external field depends on the magnetization state of the sample:[50,53] In a ZFC sample, each resonance line splits into two, one line moving to $\omega_0+\gamma_N B_z$ and the other to $\omega_0-\gamma_N B_z$. Conversely, in a FC sample, only one line is observed, shifting to higher or lower frequency depending on the direction of B_z relative to the magnetization direction. Therefore, by measuring the intensity of the shifted lines in a moderate longitudinal field, typically $\sim$0.5 T, we can check the magnetization of the sample, *as seen by the nuclei that contribute to the NMR signal*.

III. NUCLEAR SPIN DYNAMICS

A. NMR spectra

The basic feature of the ^{55}Mn NMR spectra in Mn_{12}-ac is the presence of three well-separated lines that can be ascribed to three crystallographically inequivalent Mn sites in the molecule. The $Mn^{(1)}$ line, centered around $\nu_1 \approx 230$ MHz, originates from the nuclei that belong to the central core of Mn^{4+} ions, whereas the $Mn^{(2)}$ and $Mn^{(3)}$ lines, centered at $\nu_2 \approx 280$ and $\nu_3 \approx 365$ MHz, respectively, have been assigned to the nuclei in the outer crown of Mn^{3+} ions.[49,50] In Fig. 4, we show the $Mn^{(1)}$ and $Mn^{(2)}$ spectra at $T=20$ mK, both in the oriented powder and in the single crystal, in a FC sample. Note that whereas single-crystal spectra of Mn_{12}-ac have been recently published,[40] the present spectra are the only ones measured at subkelvin temperatures so far. As argued already in Ref. 40, the single-crystal spectra indicate that the width of the $Mn^{(1)}$ line may not originate from a small quadrupolar splitting. Instead, at least two inequivalent Mn^{4+} sites may exist, supporting the growing amount of evidence about the lack of symmetry of the Mn_{12}-ac compound.

We also note that the highest peak in the $Mn^{(2)}$ line at $T=20$ mK is found at a frequency $\nu_2 \approx 287$ MHz about 8 MHz higher than most of the previously reported spectra at $T>1$ K,[40,49,50] with the exception of Ref. 54, whereas the position of the $Mn^{(1)}$ line is consistent with all the previous reports.

B. Longitudinal spin relaxation in zero field

The LSR rate as a function of temperature for the $Mn^{(1)}$ line, in zero-field and zero-field-cooled (ZFC) sample, is shown in Fig. 5. The most prominent feature in these data is a sharp crossover at $T\simeq 0.8$ K between a roughly exponential T dependence and an almost T-independent plateau. We have previously attributed the T-independent nuclear relaxation to the effect of tunneling fluctuations within the ground doublet of the cluster spins,[23] and we shall dedicate most of the present paper to discuss our further results supporting this statement. Here, we shall also argue that even in the high-temperature regime, thermally assisted quantum tunneling plays an essential role, and the experimental results cannot be understood simply in terms of LSR driven by intrawell electronic transitions.[49] It should be noted that the

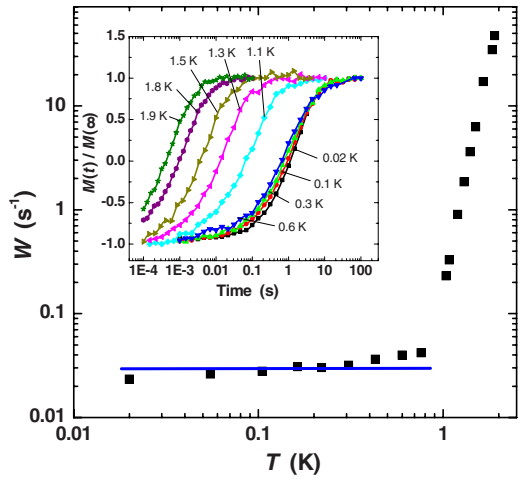

FIG. 5. (Color online) Temperature dependence of the nuclear spin-lattice relaxation rate W of the $Mn^{(1)}$ line, in zero external field and ZFC sample. The inset shows some examples of recovery of the nuclear magnetization after time t from an inversion pulse at the indicated temperatures. These curves have been fitted to Eq. (2) to extract W.

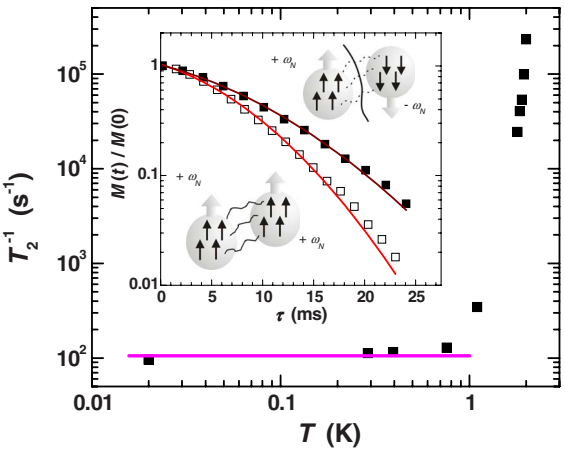

FIG. 6. (Color online) Temperature dependence of the TSR rate T_2^{-1} (squares) rates for a ZFC sample in zero field and $\nu = 231$ MHz. The solid line in the T-independent regime is a guide for the eye. Inset: normalized decay of transverse nuclear magnetization, $M(\tau)/M(0)$, for ZFC (full squares) and FC (open squares) sample at $T=20$ mK. The solid lines are fits to Eq. (4), yielding the ratio $T_{2G}^{-1}(\mathrm{FC})/T_{2G}^{-1}(\mathrm{ZFC}) = 1.35 \simeq \sqrt{2}$. The sketches in the inset represent pictorially the fact that intercluster spin diffusion is possible in a FC sample since all the nuclei have the same Larmor frequency, contrary to the case of a ZFC sample.

crossover from thermally activated to ground-state tunneling has also been observed by analyzing the T dependence of the steps in the magnetization hysteresis loops.[55,56] The important advantage of our NMR measurements is that the nuclear dynamics is sensitive to *fluctuations* of the cluster electron spins without even requiring a change in the macroscopic magnetization of the sample. Clearly, no macroscopic probe (except perhaps an extremely sensitive magnetic noise detector) would be able to detect the presence of tunneling fluctuations in a zero-field-cooled sample in zero external field since the total magnetization is zero and remains so. Below $T \sim 1.5$ K, the steps in the hysteresis loops of Mn_{12}-ac can be observed only at relatively high values of external field,[55,56] which means that the spin Hamiltonian under those conditions is radically different from the zero-field case. Therefore, that both our data and the previous magnetization measurements show a crossover around $T \simeq 0.8$ K should be considered as a coincidence.

The roughly T-independent plateau in the LSR rate below $T \simeq 0.8$ K is characterized by a value of $W \simeq 0.03$ s^{-1}, which is surprisingly high, which at first sight may appear like an argument against the interpretation in terms of tunneling fluctuations of the electron spin. Experimentally it is indeed well known[57] that the relaxation of the magnetization in Mn_{12}-ac in zero field may take years at low T, which means that the tunneling events are, in fact, extremely rare. Based on this, we are forced to assume that tunneling takes place only in a small minority of the clusters and that some additional mechanism takes care of the relaxation of the nuclei in molecules that do not tunnel. This is a very realistic assumption since all samples of Mn_{12}-ac are reported to contain a fraction of FRMs,[45,46] as mentioned in Sec. II A. Moreover, since we are also able to monitor the sample magnetization, we verified that, e.g., a FC sample maintains indeed its saturation magnetization for several weeks *while nuclear relaxation experiments are being performed (at zero field)*. This confirms that any relevant tunneling dynamics must originate from a small minority of molecules. On the other hand, it also means that the observed NMR signal comes mainly from nuclei belonging to frozen molecules; thus, there must be some way for the fluctuations in FRMs to influence the nuclear dynamics in the majority of slow molecules as well. One possibility is to ascribe it to the fluctuating dipolar field produced by a tunneling FRM at the nuclear sites of neighboring frozen molecules. In that case, we may give an estimate of W using an expression of the form

$$W \approx \frac{\gamma_N^2}{4} b_{\mathrm{dip}}^2 \frac{\tau_T}{1+\omega_N^2\tau_T^2} \approx \frac{b_{\mathrm{dip}}^2}{4B_{\mathrm{tot}}} \tau_T^{-1}, \tag{6}$$

where b_{dip} is the perpendicular component of the fluctuating dipolar field produced by a tunneling molecule on its neighbors and τ_T^{-1} is the tunneling rate. The highest value that b_{dip} may take is ~ 3 mT in the case of nearest neighbors, which leads to the condition $W \simeq 0.03$ $s^{-1} \Rightarrow \tau_T^{-1} \gg 10^6$ s^{-1}. Such a high rate is, of course, completely unrealistic. We must therefore consider the effect of a tunneling molecule on the nuclei that *belong* to the molecule itself and look for some additional mechanism that links nuclei in FRMs with equivalent nuclei in frozen clusters. It is natural to seek the origin of such a mechanism in the intercluster nuclear spin diffusion, and in the next section we shall provide strong experimental evidences to support this interpretation.

C. Transverse spin relaxation

The T dependence of the TSR rate $T_2^{-1}(T)$ is shown in Fig. 6. One may observe that below 0.8 K, the TSR—just like the LSR—saturates to a nearly T-independent plateau. In par-

ticular, $T_2^{-1}(T<0.8\ \mathrm{K}) \approx 100\ \mathrm{s}^{-1}$, which is a factor of ~3000 larger than the low-T limit of the LSR rate W. The values plotted in Fig. 6 are all obtained by fitting the decay of the transverse magnetization with Eq. (3), i.e., with a single exponential. While this is very accurate at high T, we found that for $T \lesssim 0.2$ K a better fit is obtained by including a Gaussian component, as in Eq. (4). In any case, the single-exponential fit does capture the relevant value for T_2^{-1} at all temperatures.

A point of great interest is the measurement of the TSR at $T=20$ mK in a FC and a ZFC sample, as shown in the inset of Fig. 6. The decay of the transverse magnetization is best fitted by Eq. (4), whereby the Gaussian component T_{2G}^{-1} is separated from the Lorentzian one, T_{2L}^{-1}. From the Gaussian component of the decay, we can extract directly the effect of the nuclear dipole-dipole interaction, whereas the other mechanisms of dephasing (e.g., random changes in the local field due to tunneling molecules) contribute mainly to the Lorentzian part. The fit yields $T_{2G}^{-1}(\mathrm{FC}) = 104 \pm 3\ \mathrm{s}^{-1}$ and $T_{2G}^{-1}(\mathrm{ZFC}) = 77 \pm 3\ \mathrm{s}^{-1}$. These results can be understood by assuming that, at very low T, the main source of TSR is the dipole-dipole coupling of like nuclei in neighboring molecules. Then, we can estimate T_2^{-1} from the Van Vleck formula for the second moment $M_2 = \langle \Delta\omega^2 \rangle$ of the absorption line in dipolarly coupled spins,[58]

$$M_2 = \left(\frac{\mu_0}{4\pi}\right)^2 \frac{3}{4} \gamma_N^4 \hbar^2 I(I+1) \sum_{i>j} \frac{(1-3\cos^2\theta_{ij})^2}{r_{ij}^6},$$

$$T_2^{-1} = \sqrt{M_2}, \tag{7}$$

yielding $T_2^{-1} = 131\ \mathrm{s}^{-1}$ if we take for r_{ij} the distance between centers of neighboring molecules. The estimated T_2^{-1} would obviously be much larger if one would consider the coupling between nuclei within the same cluster. As we argued when discussing the ^{55}Mn spectra, it is possible that the cluster symmetry is low enough to prevent intracluster nuclear spin flip-flops. This may explain why Eq. (7) yields the right order of magnitude when only coupling between nuclei in neighboring molecules is considered. An alternative argument is that, given the small number (4 at best) of like ^{55}Mn spins within one cluster, the dipolar coupling between them does not yield a genuine decay of the transverse magnetization for the entire sample. The macroscopic T_2 decay measured in the experiment reflects therefore the slower, but global, intercluster spin diffusion rate. A similar observation was recently made also in a different molecular compound, $Al_{50}C_{120}H_{180}$ (Ref. 59).

We also note that in the case of a ZFC sample, the sum in Eq. (7) should be restricted to only half of the neighboring molecules since, on average, half of the spins have resonance frequency $+\omega_N$ and the other half $-\omega_N$, and no flip-flops can occur between nuclei experiencing opposite hyperfine fields. This is equivalent to diluting the sample by a factor of 2, which reduces the expected T_2^{-1} in the ZFC sample by a factor of $\sqrt{2}$. Indeed, we find in the experiment $T_{2G}^{-1}(\mathrm{FC})/T_{2G}^{-1}(\mathrm{ZFC}) = 1.35 \simeq \sqrt{2}$, which, together with the good quantitative agreement with the prediction of Eq. (7), constitutes solid evidence for the presence of intercluster nuclear spin diffusion. This is precisely the mechanism required to explain why the tunneling in a minority of FRMs can relax the whole nuclear spin system. The need for intercluster nuclear spin diffusion could already have been postulated by analyzing the LSR rate, and the magnetization dependence of the TSR rate gives an independent confirmation.

For comparison, in a recent study of the ^{57}Fe NMR in Fe_8, Baek *et al.*[26] attributed the observed TSR rate to the dipolar interaction between ^{57}Fe and ^{1}H nuclei. They analyzed their data with the expression $T_2^{-1} \simeq (M_2^{(\mathrm{H})}/12\tau_c)^{1/3}$, where τ_c is the proton TSR time due to their mutual dipolar coupling and $M_2^{(\mathrm{H})}$ is the second moment of the ^{57}Fe-^{1}H coupling. However, the same model[60] predicts the echo intensity to decay as $M_\perp(t)/M_\perp(0) \simeq \exp(-2M_2^{(\mathrm{H})}t^3/3)$. This function fails completely in fitting our echo decays; therefore, we do not consider the ^{55}Mn-^{1}H dipolar coupling as an alternative explanation for the TSR we observe.

Finally, we stress that, in our view, the fact that the LSR and the TSR are both roughly T independent below 0.8 K does not find its origin in the same mechanism. Rather, we attribute them to two different mechanisms, both T independent: the quantum tunneling of the electron spin (for the LSR) and the nuclear spin diffusion (for the TSR).

Having argued that the LSR in Mn_{12}-ac is driven by tunneling fluctuations of the FRMs, which are peculiar of the acetate compound, it is interesting to note that other varieties of Mn_{12} molecules have meanwhile become available. In particular, Mn_{12}-tBuAc (Ref. 61 and 62) is a truly axially symmetric variety that does not contain any FRMs and could provide an interesting counterexample for our results if studied by low-T NMR. The Mn_{12}BrAc molecule is also thought to be free of FRMs,[40] and some low-T NMR experiments have been performed on it[27] that show indeed very different results from what we report here. However, as we shall argue in Sec. IV, a definite conclusion on the meaning of NMR experiments at very low T should only be drawn when the analysis of the nuclear spin thermalization is included.

D. Field dependence of the longitudinal spin relaxation rate

Further insight in the interplay between the quantum tunneling fluctuations and the nuclear spin dynamics is provided by the study of the dependence of the LSR on a magnetic field B_z applied along the anisotropy axis. It is clear from the Hamiltonian [Eq. (1)] that, in the absence of other perturbations, such a longitudinal field destroys the resonance condition for electron spin states on opposite sides of the barrier and therefore inhibits the quantum tunneling. In the presence of static dipolar fields B_{dip}, by studying the tunneling rate as a function of B_z one may, in principle, obtain information about the distribution of longitudinal B_{dip} since at a given value of B_z there will be a fraction of molecules for which $B_{\mathrm{dip}} = -B_z$ and will therefore be allowed to tunnel just by the application of the external bias.

We show in Fig. 7 the LSR rate $W(B_z)$ at $T=20$ mK in the ZFC sample, obtained while shifting the measurement frequency as $\nu(B_z) = \nu(0) + \gamma_N B_z$, with $\nu(0) = 230$ MHz, in order to stay on the center of the NMR line that corresponds to the molecules that are aligned exactly parallel with the applied

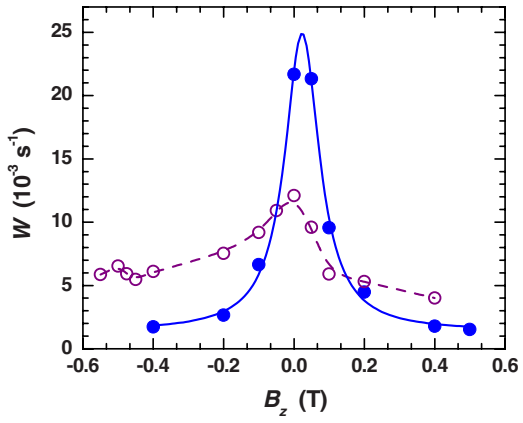

FIG. 7. (Color online) Longitudinal field dependence of the LSR rate W in the ZFC (solid dots) and FC (open dots) sample at $T=20$ mK. The measuring frequencies are $\nu(B_z)=230+\gamma_N B_z$ MHz. The solid line is a Lorentzian fit with HWHM $\Delta B_z \simeq 60$ mT. The dotted line through the FC data is a guide for the eye.

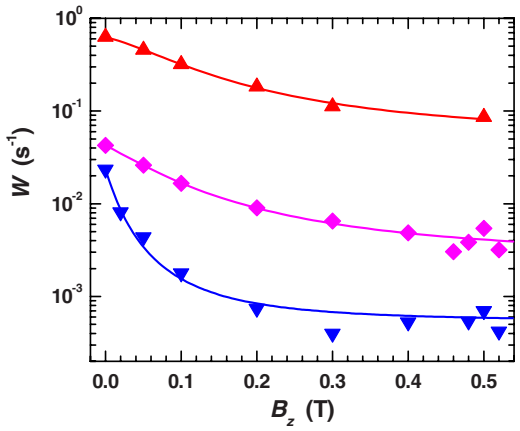

FIG. 8. (Color online) Longitudinal field dependence of the LSR rate in ZFC sample at $T=20$ mK (down triangles), $T=720$ mK (diamonds), and $T=1.13$ K (up triangles). The measuring frequency in these data sets is $\nu=231+\gamma_N B_z$ MHz. The lines are Lorentzian fits yielding HWHM $\Delta B_z=16$, 85, and 118 mT, respectively.

field. Since for a ZFC sample the magnetization is zero, the field dependence should be the same when B_z is applied in opposite directions, as is observed. The data can be fitted by a Lorentzian with a half-width at half maximum (HWHM) $\Delta B_z \simeq 60$ mT: This differs both in shape (Gaussian) and in width ($\Delta B_z \simeq 21$ mT) from the calculated dipolar bias distribution in a ZFC sample.[63] An alternative experimental estimate, $\Delta B_z \simeq 25$ mT, can be found in magnetization relaxation experiments,[45] but only around the first level crossing for FRMs ($\simeq 0.39$ T) in the FC sample. For comparison, Fig. 7 also shows $W(B_z)$ in the FC sample: The shape is now distinctly asymmetric, with faster relaxation when the external field is opposed to the sample magnetization. Interestingly, $W(B_z)$ in the FC sample falls off much more slowly on the tails for both positive and negative fields, while the value at zero field is less than half that for the ZFC sample. We therefore observe that in zero field the recovery of longitudinal magnetization in the FC sample is faster than in the ZFC, whereas the opposite is true for the decay of transverse magnetization (inset of Fig. 6).

If the LSR rate $W(B_z)$ is to be interpreted as a signature of quantum tunneling, its HWHM is clearly larger than expected. Part of the reason may be the fact that the width of the $Mn^{(1)}$ line is already intrinsically larger than both ΔB_z and the distribution of dipolar fields created by the molecules. Indeed, the width of the $Mn^{(1)}$ line, $\sigma_\nu \simeq 1.2$ MHz, translates into a local field distribution of width $\sigma_B \simeq 115$ mT for ^{55}Mn. The observed HWHM does depend, for instance, on the choice of $\nu(0)$. As soon as $B_z \neq 0$, the presence of slightly misaligned crystallites in our sample may also contribute to the width of the resonance. In any case, all of the mechanisms mentioned above (distribution of internal dipolar fields, width of the NMR line, distribution of crystallite orientations in the sample) would yield a T-independent linewidth for $W(B_z)$. Figure 8 shows $W(B_z)$ in the ZFC sample at three different temperatures, $T=0.02$, 0.72, and 1.13 K, covering the pure quantum regime, the thermally activated regime, and the crossover temperature. The NMR frequency in these data sets is $\nu(B_z)=231+\gamma_N B_z$. The data have been fitted by Lorentzian lines yielding a HWHM $\Delta B_z=16$, 85, and 118 increasing with temperature. We note immediately that the HWHM at $T=20$ mK is much smaller than the one obtained from the data in Fig. 7, the only difference between the two sets being $\nu(0)$ and, subsequently, all other measurement frequencies at $B_z \neq 0$. Indeed, we found that in zero field the LSR rate does depend on ν, reaching the highest values at the center of the line and falling off (up to a factor of 5) on the sides. This dependence, however, becomes much weaker at high temperatures. It is therefore rather difficult to make strong statements about the meaning of the observed increase in ΔB_z with temperature. At any rate, however, the field dependencies observed here at low T are much stronger than those previously reported in the high-T regime.[24,49] Goto *et al.* also reported $W(B_z)$ for the "lower branch" of the $Mn^{(1)}$ line, viz., for the nuclei whose local hyperfine field is opposite to the external field (Ref. 24, Fig. 6, closed squares). That situation is equivalent to our FC data (Fig. 7, open dots) for $B_z<0$. At large fields, an overall increase of W with B_z is observed in Ref. 24, but for $B_z<1$ T the LSR rate does decrease, in agreement with our results.

We also noted, both in Fig. 8 and in the FC data in Fig. 7, that a small increase in $W(B_z)$ occurs at $|B_z| \simeq 0.5$ T, which is approximately the field value at which the $|+9\rangle$ and $|-10\rangle$ electron spin states come into resonance. This feature is barely observable, but nevertheless well reproducible. As a counterexample, in another data set (not shown), we investigated $W(B_z)$ more carefully in the FC sample at $T=20$ mK for positive values of B_z, and found no increase at around $B_z \simeq 0.5$ T, as one would expect since the fully populated state, $|-10\rangle$, is pushed far from all other energy levels. A similarly small peak in $W(B_z)$ at the first level crossing has been recently observed in Fe_8 as well.[26]

E. Deuterated sample

The role of the fluctuating hyperfine bias on the incoherent tunneling dynamics of SMMs, predicted by Prokof'ev

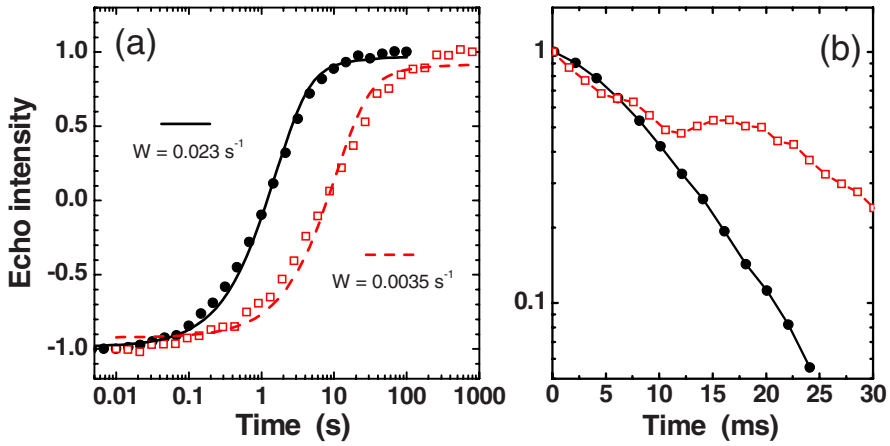

FIG. 9. (Color online) Comparison between (a) the nuclear inversion recoveries and (b) the decays of transverse magnetization in the "natural" Mn_{12}-ac (circles) and in the deuterated sample (squares) at $T=20$ mK in zero-field and ZFC sample for the $Mn^{(1)}$ site. The solid lines in (a) are fits to Eq. (2).

and Stamp,[6] has been clearly demonstrated by measuring the quantum relaxation of the magnetization in Fe_8 crystals in which the hyperfine couplings had been artificially modified by substituting ^{56}Fe by ^{57}Fe or ^{1}H by ^{2}H (Ref. 18). For instance, the time necessary to relax 1% of the saturation magnetization below 0.2 K was found to increase from 800 to 4000 s by substituting protons by deuterium, whereas it decreased to 300 s in the ^{57}Fe enriched sample. More recently, Evangelisti *et al.*[19] showed that the ^{57}Fe isotopic enrichment of Fe_8 causes the magnetic specific heat to approach its equilibrium value within accessible time scales ($\sim$100 s).

Since in Mn_{12}-ac the only possible isotope substitution is $^{1}H \rightarrow {}^{2}H$, we performed a short set of measurements on a deuterated sample. The sample consists of much smaller crystallites than the "natural" ones used in all other experiments reported here. Although a field alignment was attempted following the same procedure, as described in Sec. II C, the orientation of the deuterated sample turned out to have remained almost completely random, probably due to the too small shape anisotropy of the crystallites. We therefore report only experiments in zero external field, where the orientation is, in principle, irrelevant.

The results are shown in Fig. 9: The ^{55}Mn LSR rate at $T=20$ mK in zero-field and ZFC sample is indeed reduced to $W_{deut} \simeq 0.0035$ s^{-1}, i.e., 6.5 times lower than in the natural sample. This factor is the same as the reduction of the electron spin relaxation rate seen in deuterated Fe_8 (Ref. 18), and it coincides with the ratio of the gyromagnetic ratios of ^{1}H and ^{2}H. This finding unequivocally proves that the proton spins are very effective in provoking the tunneling events via the Prokof'ev-Stamp mechanism and confirms that the LSR rate of the ^{55}Mn nuclei is a direct probe of the electron spin tunneling rate.

As regards the TSR, the result is quite intriguing: Slow but rather ample oscillations are superimposed to the decay of transverse magnetization, and the overall decay rate appears slower than in the natural sample. This behavior is reminiscent of the change in TSR rate upon application of a small longitudinal magnetic field in the natural sample. The latter has a rather complicated physical origin and is still under investigation.

F. Comparison with a Mn^{3+} site

Some rather interesting results emerge from the analysis of extra measurements performed on the NMR line of the $Mn^{(2)}$ site, i.e., a Mn^{3+} ion. Figure 10 shows a comparison between the recovery of the longitudinal magnetization and the decay of the transverse magnetization in $Mn^{(1)}$ and $Mn^{(2)}$ sites, at $T=20$ mK in the FC sample and zero external field, at a frequency $\nu^{(2)}=283.7$ MHz. The TSR is very similar in both sites, although a closer inspection evidences that the Gaussian nature of the decay is less pronounced in the $Mn^{(2)}$ sites, which leads to $T_{2G}^{-1}=83$ s^{-1} instead of the $T_{2G}^{-1}=104$ s^{-1} found in $Mn^{(1)}$. More importantly, the LSR is three times slower in the $Mn^{(2)}$ site, as seen in Fig. 10(b). This is opposite to the high-T regime, where the Mn^{3+} sites were found[24,49] to have much faster relaxation. Furthermore, the field dependence of the LSR rate appears sharper in the $Mn^{(2)}$ site, as shown in Fig. 11. The asymmetry in $W(B_z)$ for a FC sample is still present, but less evident than in the $Mn^{(1)}$ site due to the more pronounced decrease of W for small applied fields.

The similarity between the TSR rates in the $Mn^{(1)}$ and $Mn^{(2)}$ sites is indeed expected if T_2 is determined by intercluster nuclear spin diffusion. Conversely, the difference in LSR is more difficult to understand if one assumes that the process that induces longitudinal spin relaxation is the tunneling of the molecular spin. However, one clear difference between $Mn^{(1)}$ and $Mn^{(2)}$ is the width of the NMR line, much larger in $Mn^{(2)}$. Since the integrated intensity of both lines is identical, the $Mn^{(2)}$ has an accordingly lower maximum intensity. We have verified for both sites that the LSR rate is the fastest when measuring at the highest intensity along each line. Thus, the factor of 3 slower LSR in $Mn^{(2)}$ could simply be another manifestation of the apparent dependence of the measured W on the NMR intensity along each line. We point out, however, that the measured LSR rate is independent of the $\pi/2$ pulse length, which determines the spectral

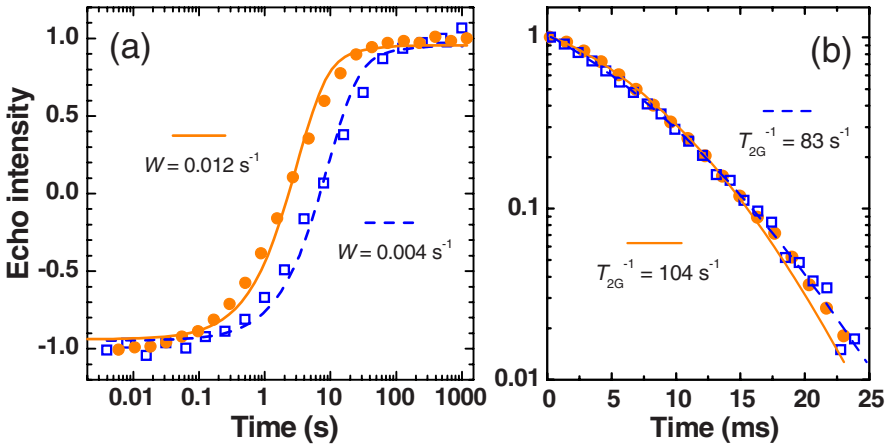

FIG. 10. (Color online) Comparison between (a) the recovery of longitudinal magnetization and (b) the decay of transverse magnetization in $Mn^{(1)}$ (circles) and $Mn^{(2)}$ (diamonds) sites at $T=20$ mK in FC sample and zero external field. The solid ($Mn^{(2)}$) and dashed ($Mn^{(1)}$) lines are fits to Eq. (2) in panel (a) and to Eq. (4) in panel (b).

width of the pulse and thereby the fraction of spins being manipulated and observed. This means that the difference in W for the two sites cannot be simply attributed to a difference in the number of spins excited during a pulse of given length but that other (more complex) factors must play a role.

IV. THERMALIZATION OF THE NUCLEAR SPINS

Having demonstrated that the ^{55}Mn longitudinal spin relaxation below 0.8 K is driven by T-independent quantum tunneling fluctuations, a natural question to ask is whether or not the nuclear spins are in thermal contact with the lattice at these low temperatures. Let us recall that any direct coupling between phonons and nuclear spins is expected to be exceedingly weak due to the very small density of phonons at the nuclear Larmor frequency.[64] Relaxation through electric quadrupole effects, if present, would show a temperature dependence $\propto(T/\Theta_D)$ for a direct process or $\propto(T/\Theta_D)^2$ for a Raman process (Θ_D is the Debye temperature), which is not consistent with our observations. Therefore, the thermalization of the nuclei will have to take place via the electron spin–lattice channel. Since in the quantum regime the only electron spin fluctuations are due to tunneling, the question of whether the nuclear spins will still be in equilibrium with the lattice temperature is of the utmost importance.

A. Time evolution of the nuclear spin temperature

We have addressed this problem by cooling down the refrigerator from 800 to 20 mK while monitoring simultaneously the temperature $T_{\rm bath}$ of the ^{3}He/^{4}He bath in the mixing chamber (just next to the sample) and the NMR signal intensity of the $Mn^{(1)}$ line, in zero external field and on a ZFC sample. The signal intensity was measured by spin echo with repetition time $t_{\rm rep}=60$ s. The nuclear spin temperature[65] $T_{\rm nucl}$ is obtained, as described in Sec. II C, and plotted in Fig. 12 together with $T_{\rm bath}$. We find that the nuclear spin temperature strictly follows the bath temperature, with small deviations starting only below ~200 mK. This result is crucial but rather paradoxical, and we shall discuss its implications in detail in Sec. V D. Experimentally, however, it certifies the effectiveness of our cryogenic design in achieving the best possible thermalization of the sample since the nuclear spins are the last link in the chain going from the ^{3}He/^{4}He bath via the phonons in the sample to the electron spins and finally to the nuclei.

The lowest spin temperature that can be *measured* appears to depend on the pulse repetition time $t_{\rm rep}$. To measure $T_{\rm nucl}$ with the pulse NMR method, we need a $\pi/2$ pulse to create a transverse nuclear magnetization, and after a time T_2, the spins are effectively at infinite T so enough time must elapse before taking the next $T_{\rm nucl}$ measurement. For the data in Fig. 12, $t_{\rm rep}=60$ s was barely longer than the observed time for inversion recovery [see Fig. 3(b)], and the lowest observed spin temperature is $T_{\rm nucl}^{\rm min}\simeq 80$ mK. This improved when using longer waiting times between pulses, e.g., $T_{\rm nucl}^{\rm min}\simeq 35$ mK with $t_{\rm rep}=180$ s, as shown in the inset of Fig. 12.

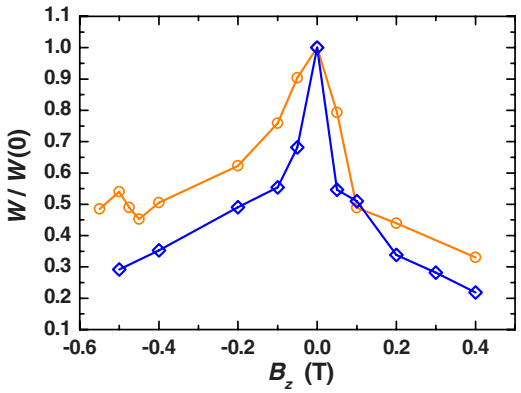

FIG. 11. (Color online) Longitudinal field dependencies of the LSR rates in $Mn^{(1)}$ (circles) and $Mn^{(2)}$ (diamonds) sites, normalized at the zero-field value. The data are taken at $T=20$ mK in the FC sample with central measuring frequencies $\nu^{(1)}(0)=230$ MHz and $\nu^{(2)}(0)=283.7$ MHz.

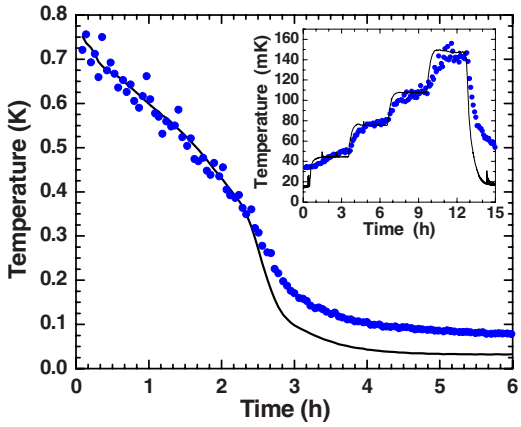

FIG. 12. (Color online) Comparison between bath temperature T_{bath} (solid lines) and nuclear spin temperature T_{nucl} (circles), while cooling down the system (main panel) and while applying steplike heat loads (inset). The waiting time between NMR pulses was 60 s in the main panel and 180 s in the inset. Both data sets are at zero field in the ZFC sample.

However, no matter how long the waiting time, we never observed a T_{nucl} lower than ~30 mK.

Next, we study the time constant τ_{th} for the thermalization of the nuclear spin system with the helium bath by applying steplike heat loads and following the time evolution of T_{nucl}. In particular, we are interested in the relationship between τ_{th}, the LSR time $T_1 = 1/2W$, as obtained from the inversion recovery technique, and the ^{3}He circulation rate $\dot{n}$, which is proportional to the refrigerator's cooling power $\dot{Q}$. T_1 is easily tuned by measuring at different longitudinal fields and Mn sites, while $\dot{n}$ is changed by applying extra heat to the refrigerator still. Since also the NMR signal intensity changes under different fields and Mn sites, we must redefine every time the conversion factor K between signal intensity and T_{nucl}. In the following, we choose K such that the asymptotic value of T_{nucl} for $t \to \infty$ matches the measured T_{bath} at the end of the heat step. This implies the assumption that the measuring pulses do not saturate, i.e., "heat up," the nuclear spins, and requires $T_{rep} > T_1$. Figure 13 shows four examples of the time evolution of T_{nucl} under the application of a heat load for ~2 h, in $Mn^{(1)}$ and $Mn^{(2)}$ sites, with or without an applied field and with an increased ^{3}He flow rate. We fitted the data to the phenomenological function,

$$T_{nucl}(t) = T_{nucl}(0) + [T_{nucl}(\infty) - T_{nucl}(0)]\left[1 - \exp\left(-\frac{t - t_0}{\tau_{th}}\right)\right], \tag{8}$$

where $T_{nucl}(\infty)$ is set by a definition equal to T_{bath} at the end of the step, $T_{nucl}(0)$ follows automatically from the above

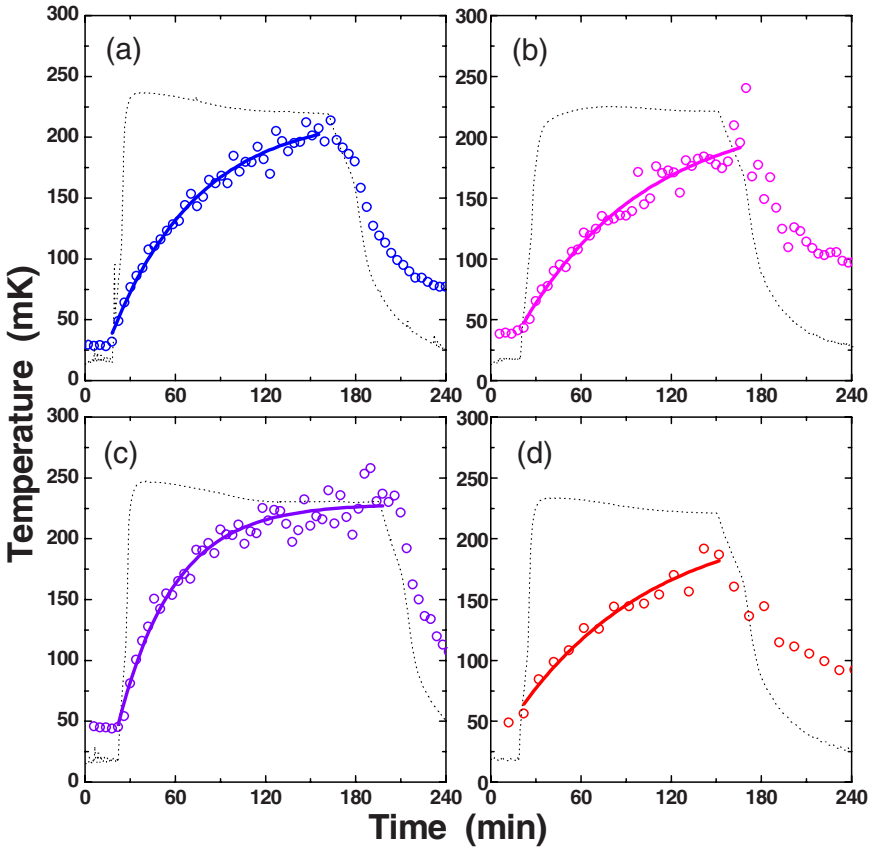

FIG. 13. (Color online) Time evolution of the nuclear spin temperature (open symbols) and the bath temperature (dotted lines) upon application of a steplike heat load. All data are for a FC sample. The solid lines are fits to Eqs. (9a) and (9b), yielding the thermal time constants τ_{th} reported in Table I, along with the Mn site, external magnetic field B_z, LSR rate W, NMR pulse repetition time t_{rep}, ^{3}He flow rate $\dot{n}$, and applied heat load $\dot{Q}$. Notice, in particular, the effect of a change in ^{3}He circulation rate, panel (c) vs panel (a).

TABLE I. Experimental conditions and relaxation rates for the nuclear spin temperature experiments in Fig. 13

Panel	Mn site	B_z (T)	$\dot{n}$ (μmol/s)	$\dot{Q}$ (mW)	t_{rep} (s)	T_1 (s)	τ_{th} (min)
(a)	1	0	330	0.63	120	41.3	58±5
(b)	2	0	330	0.63	120	122	83±13
(c)	1	0	430	0.78	120	41.3	37±3
(d)	2	0.2	330	0.63	300	355	92±33

constraint, and t_0 is the time at which the heat pulse is started. We find that τ_{th} is always much longer than the nuclear LSR time T_1 and that larger T_1 corresponds to larger τ_{th}. However, the dependence of τ_{th} on the Mn site and applied field is not as strong as for T_1; i.e., τ_{th} and T_1 are not strictly proportional to each other. Conversely, by changing the ^{3}He flow rate we observe that, within the errors, the ratio of heat transfer from the ^{3}He stream to the nuclear spins is proportional to $\dot{n}$, given the same conditions of nuclear site and external field.

We should stress that when measuring T_1 by inversion recovery, we effectively heat up only a small fraction of the nuclear spins, namely, those whose resonance frequencies are within a range, $\delta\nu$, proportional to the inverse of the duration, t_π, of the π pulse. With $t_\pi \simeq 20$ μs, we get $\delta\nu = 1/2\pi t_\pi \simeq 8$ KHz, which is less than 0.2% of the width of the $Mn^{(1)}$ line. Conversely, by increasing the bath temperature, we heat up the entire spin system, thereby requiring a much larger heat flow to occur between the ^{3}He stream and the nuclear spins. Therefore, these results show that the thermal equilibrium between nuclear spins and lattice phonons does occur on a time scale of the order of T_1, as obtained from inversion recovery, since the main bottleneck appears to be between lattice phonons and ^{3}He stream, as demonstrated by the dependence of τ_{th} on $\dot{n}$. In a later set of experiments (not shown here) using a small single crystal instead of a large amount of oriented powder, we have indeed observed an even shorter τ_{th}, which indicates that τ_{th} should ultimately tend to T_1 for a small sample size and a strong thermal contact between lattice phonons and helium bath.

B. Longitudinal field sweeps and magnetic avalanches

To conclude our study on the nuclear spin thermalization, we attempted to measure T_{nucl} in the presence of large longitudinal magnetic field sweeps, motivated by the fact that much of the experiments on spin tunneling in SMMs are based on the measurement of magnetic hysteresis loops. Under those conditions, the electron spins are flipped at abnormally large rates, and one may ask whether or not the nuclear spins are still able to remain in thermal equilibrium. Unfortunately, monitoring T_{nucl} while B_z is being swept means that one should continuously change the NMR probe frequency and synchronize that change with the field sweep. This being technically cumbersome, we could only measure T_{nucl} at zero field at the beginning and at the end of a B_z sweep. The results are somewhat inconclusive and shall not be discussed here, but more details can be found in Sec. 4.4.2 of Ref. 48.

We do mention, however, that during the B_z-sweep experiments we always encountered magnetic avalanches, i.e., abrupt reversal of the electronic magnetization of the whole sample. This phenomenon has been first reported some time ago,[66] but is only recently being studied in more detail.[67] Importantly, the magnetization reversal is expected to be accompanied by the emission of electromagnetic radiation,[68] which is, in fact, what we observed in our experiments, since we were not equipped to measure the electronic magnetization directly on short time scales. Figure 14 shows the temperature recorded by the upper thermometer in the mixing chamber (see Fig. 2) while the longitudinal field is being swept at a rate of $dB_z/dt = 0.5$ T/min. The sweeping field gives a heat load that raises the observed temperature to $\simeq 30$ mK, but the most striking feature of the data is the sudden jump of T_{upper} to above 100 mK whenever the applied field reaches $|B_z| \simeq 1.9$ T *and* its direction is opposite to the instantaneous magnetization. We note that the time scale for the apparent temperature jump is essentially identical to what we observed immediately after the application of a rf pulse for NMR measurements, as shown in Fig. 2(b). In the same figure it is seen that a heat pulse applied at the sample location shows its effect at the upper thermometer with a

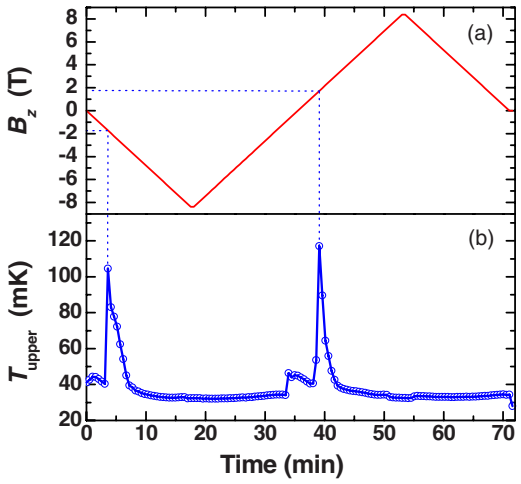

FIG. 14. (Color online) (a) Longitudinal magnetic field and (b) temperature of the upper thermometer (see Fig. 2) during a field sweep at $dB_z/dt = 0.5$ T/min. The sample was initially field cooled with $B_z > 0$. The sharp jumps in T_{upper} occur when $|B_z| \simeq 1.9$ T, i.e., at the fourth level crossing field, and are attributed to the radiation produced by a magnetic avalanche.

delay of about 3 min (due to the ^{3}He drift velocity) in the form of a broad temperature "bump." We therefore conclude that the sudden jumps in $T_{\rm upper}$ shown in Fig. 14(b) must be of *electromagnetic* rather than *thermal* origin, and may be attributed to the radiation produced by the sudden reversal of the entire electronic magnetization of the sample by the magnetic avalanche.[68] The radiation bursts reported in Ref. 68 at a temperature $T=1.8$ K occurred at $|B_z^{(\rm av)}|\simeq 1.4$ T, which corresponds to the third level crossing field for spin tunneling, i.e., the value of field at which the resonance between $m=\pm 10$ and $m=\mp 7$ states is obtained. We found instead the avalanches at $|B_z^{(\rm av)}|\simeq 1.9$ T, i.e., the fourth level crossing, $m=\pm 10\leftrightarrow\mp 6$, but our measurements are done at $T\simeq 30$ mK. Goto *et al.*[69] also reported the observation of magnetic avalanches in Mn_{12}-ac, and studied the temperature dependence of the avalanche field $B_z^{(\rm av)}$. Their finding that $B_z^{(\rm av)}$ increases with temperature was interpreted as a sign that the avalanches occur more easily when the thermal contact to the bath is weaker. Indeed, whereas they would observe avalanches even at fields as low as $B_z^{(\rm av)}\simeq 0.5$ T (the first level crossing), with the sample loosely anchored to the mixing chamber of a dilution refrigerator at $T=0.15$ K, they never saw avalanches when the same sample was placed directly in a liquid helium bath at $T=1.4$ K. In this sense, our observation of a high $B_z^{(\rm av)}\simeq 1.9$ T confirms once more that our strategy for the sample thermalization is very effective. Suzuki *et al.*[67] found even higher values of $B_z^{(\rm av)}$ at subkelvin temperatures when measuring the local magnetization of a small Mn_{12}-ac crystal immersed in liquid ^{3}He. However, their observations differ markedly from ours in that they found avalanches occurring in a wide range of (not necessarily resonant) fields, whereas we saw avalanches always and only at the fourth level crossing field.

V. ANALYSIS OF THE NUCLEAR SPIN DYNAMICS AND THEORETICAL IMPLICATIONS

In this section, we attempt a quantitative analysis of our experimental results, particularly the observed values of LSR rate. To this end, we shall apply the Prokof'ev-Stamp (PS) theory of the spin bath, which describes the dynamics of a central spin **S** (here, the giant electronic spin of a Mn_{12}-ac cluster) coupled to a bath of environmental (in this case, nuclear) spins. In view of the complexity of the model, we provide here an introductory overview of some essential elements of the PS theory needed for our analysis, referring the reader to the original papers[5–7,70] for more details. For comparison, we also calculate the LSR rate, assuming that the electron spin tunneling is driven by spin-phonon coupling.[70,71] We anticipate that the result of this effort will be that the existing theory is not sufficient to properly describe these and other related experiments.[19,72] We shall carry out the analysis in detail in order to emphasize at every step what assumptions are being made, what is their actual validity, and why the known theories cannot explain the data.

The goal of our analysis is to link the electron spin tunneling rate $\Gamma=\tau_T^{-1}$ to the observed LSR rate W based on the following assumptions, justified by the experiments presented in the previous sections: (i) The nuclear relaxation is driven by tunneling fluctuations in a minority of fast-relaxing molecules. We shall assume the fraction of FRMs to be 5% of the total.[45] The neighboring slow molecules can be safely considered as frozen during the time scale of interest and serve simply as a "reservoir of nuclear polarization." (ii) The dipole-dipole coupling between ^{55}Mn nuclei in equivalent sites of neighboring molecules allows intercluster nuclear spin diffusion, at a rate T_2^{-1} much faster than the LSR rate. (iii) The nuclear spin system is in thermal equilibrium with the phonon bath.

Before we start, it is of interest to point out some rather striking peculiarities of the problem at hand. First and most importantly, one cannot use any result from perturbation theory here because the nuclear Zeeman splittings arise uniquely from hyperfine fields, which themselves jump between two different directions each time the electron spin of a molecule tunnels, so there is no static part of the nuclear Hamiltonian. Perhaps the only situation that resembles this is the nuclear quadrupolar relaxation in systems with molecular rotations.[73] Conversely, in the overwhelming majority of NMR experiments, one has a static external field (produced by an actual magnet) and some local fluctuating fields arising from the magnetic environment of the nuclei, which can be treated as small perturbations. Then, the LSR rate is easily related to the spectral density of the local magnetic fluctuations, calculated at the NMR frequency determined by the external field.[64,74] Also curious is the way nuclear spin diffusion proceeds in our system. The well-known treatment of nuclear relaxation by coupling to paramagnetic impurities plus nuclear spin diffusion[75] shows that there is a "spin diffusion barrier radius" below which neighboring nuclear spins cannot exchange energy because the large dipolar field from the impurity brings them out of resonance. Here, instead, there is no such minimum radius for spin diffusion because nuclei at equivalent sites of different molecules are also magnetically equivalent (provided both molecules have the same electron spin orientation).

A. Spin-bath analysis and tunneling rate

To apply the spin-bath theory to the ^{55}Mn NMR in Mn_{12}-ac, we begin by truncating the giant spin Hamiltonian of the cluster to its tunneling-split ground doublet and by taking as a basis for its subspace the $m=\pm S$ projections of **S** along the $\hat{z}$ axis, denoted by $|\Uparrow\rangle$, $|\Downarrow\rangle$. This restriction will be relaxed to consider higher excited electron spin doublets when discussing thermally assisted tunneling. Further, we assume that each central spin is coupled to N nuclear spins $\{\mathbf{I}_k\}$, $k=1,\ldots,N$. The strength of each coupling is given by the quantities $\hbar\omega_k^{\parallel}$ and $\hbar\omega_k^{\perp}$, which represent the part of the hyperfine coupling that does or does not change upon flipping the central spin, respectively (Fig. 15). For nuclei in $Mn^{(1)}$ sites of Mn_{12}-ac, the hyperfine field $\mathbf{B}_{\rm hyp}$ is exactly parallel or antiparallel to the direction of the cluster's $\hat{z}$ axis, so $\omega_k^{\perp}=0$ and $\omega_k^{\parallel}=\gamma_N B_{\rm hyp}$. In $Mn^{(2)}$ and $Mn^{(3)}$ sites, there is a small nonzero value of $\omega_k^{\perp}$ due to the orbital contribution to the hyperfine field.[50] Conversely, for nuclei, such as ^{1}H, which are subject to the vector sum of the dipolar fields from

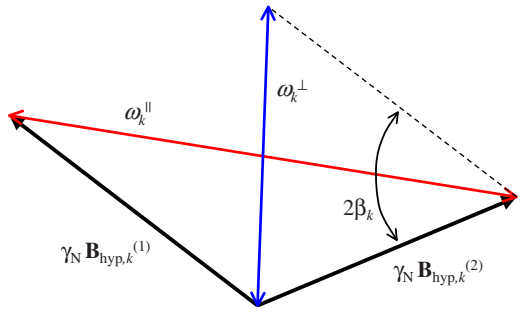

FIG. 15. (Color online) Scheme of the relative orientations of the hyperfine fields before ($\mathbf{B}_{\mathrm{hyp},k}^{(1)}$) and after ($\mathbf{B}_{\mathrm{hyp},k}^{(2)}$) the electron spin flip, and the components of the hyperfine coupling that change ($\omega_k^{\parallel}$) or stay unchanged ($\omega_k^{\perp}$) at each tunneling event. The angle β_k is involved in the definition of κ, the number of nuclei coflipping by "orthogonality blocking," Eq. (9a).

several surrounding clusters, we may expect $\omega_k^{\perp}$ and $\omega_k^{\parallel}$ to have comparable values. Let us define for each nuclear spin a number m_k representing the spin projection of $\mathbf{I}_k$ along the direction of the local hyperfine field $\mathbf{B}_{\mathrm{hyp},k}$. For ^{1}H nuclei, $m_k=\pm 1/2$, while for ^{55}Mn, $m_k=-5/2\cdots+5/2$. Then, the total hyperfine bias on the cluster is $\xi_N=-2\hbar\Sigma_{k=1}^{N} m_k\omega_k^{\parallel}$. With this definition, $\xi_N<0$ when the majority of nuclear spins is parallel to the local $\mathbf{B}_{\mathrm{hyp},k}$, thereby lowering the total energy of the system. Notice that for a given orientation of the nuclear spins, ξ_N changes sign whenever the electron spin flips since the direction of $\mathbf{B}_{\mathrm{hyp}}$ does. Thus, we define an *absolute* index of nuclear polarization in each cluster as $\mathcal{P}=C_S\Sigma_k m_k$, with $C_S=+1$ when $\mathbf{S}$ is in the $|\Uparrow\rangle$ state, and $C_S=-1$ otherwise. Each possible value of $\mathcal{P}$ defines a "polarization group" and is independent of the electron spin state. Since the individual hyperfine couplings vary over a broad range (from $\sim$1 MHz for distant protons to 365 MHz in Mn[3]), the possible values of the bias ξ_N for each $\mathcal{P}$ are also widely spread, yielding a set of largely overlapping polarization groups. Globally, we may describe the coupled "central spin+spin bath" system by two manifolds of states, one for each electron spin state $|\Uparrow\rangle$, $|\Downarrow\rangle$, split by hyperfine interactions into a dense band of states indexed by the nuclear polarization $\mathcal{P}$, as shown in Fig. 16. Calling $\mathcal{P}_{\max}$ the maximum value assumed by $\mathcal{P}$, $\mathcal{P}_{\max}=N$ if $I_k=1/2\,\forall k$. The profile of the hyperfine bias distribution can be calculated with the knowledge of the individual couplings and is well described by a Gaussian with half-width $E_0=\Sigma_k[(I_k+1)/3I_k](\omega_k^{\parallel}I_k)^2 \simeq 0.082$ K.[70]

In addition to the hyperfine couplings, the $\mathbf{S}$ spins are also mutually coupled by dipolar interactions, which yield an additional bias $\xi_D=2g\mu_B\mathbf{S}\cdot\mathbf{B}_{\mathrm{dip}}$. The dipolar bias can be considered quasistatic in the sense that it remains essentially constant over time intervals that are long compared to the typical time scale for the hyperfine bias fluctuations. The distribution of dipolar biases depends on the total magnetization of the sample and, in general, on its shape. For a demagnetized ZFC sample of Mn_{12}-ac, the dipolar bias distribution is described by a Gaussian with half-width $E_D \simeq 0.32$ K.[63] Finally, one may in general apply a static external field B_z along the $\hat{z}$ axis, which produces an additional bias $\xi_B=2g\mu_B S_z B_z$. For zero external field and some typical nonzero value of ξ_D, the energy level scheme of a Mn_{12}-ac cluster coupled to its nuclear spins would resemble the sketch shown in Fig. 16.

To analyze the behavior of this system with respect to incoherent tunneling of the electron spin, the crucial questions to be answered are: What happens to the nuclear spins when $\mathbf{S}$ suddenly changes direction? How many of the $\{\mathbf{I}_k\}$ coflip with $\mathbf{S}$? As extensively discussed in the PS literature,[5–7] there are two mechanisms by which nuclear spins may be flipped by a tunneling event. First, a nuclear spin may coflip with $\mathbf{S}$ if the local hyperfine field does not exactly reverse its direction after $\mathbf{S}$ has tunneled since it would then start to precess around a different axis, hence the name "orthogonality blocking" or "precessional decoherence" for this mechanism. The number of spins coflipped this way is κ, defined as (see Fig. 15 for β_k)

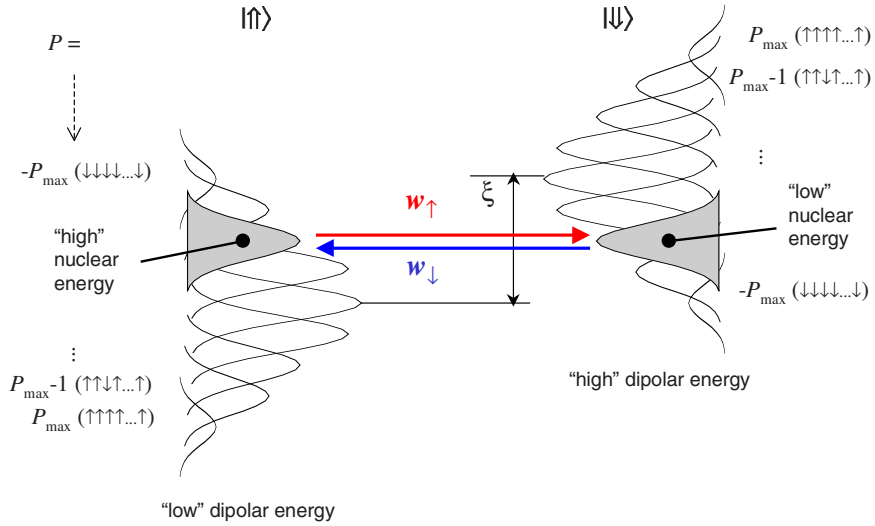

FIG. 16. (Color online) Sketch of the hyperfine-split manifolds representing the energy of the $m=\pm S$ electron spin levels coupled to the nuclear spin bath.

$$e^{-\kappa} = \prod_k \cos\beta_k \approx e^{-(1/2)\Sigma_k \beta_k^2}, \tag{9a}$$

$$\cos(2\beta_k) = \frac{-\mathbf{B}_{\mathrm{hyp},k}^{(1)} \cdot \mathbf{B}_{\mathrm{hyp},k}^{(2)}}{|\mathbf{B}_{\mathrm{hyp},k}^{(1)}||\mathbf{B}_{\mathrm{hyp},k}^{(2)}|}. \tag{9b}$$

The cosine factors in Eq. (9a), which are multiplied over all the bath spins, are the overlap matrix elements between the initial and final bath states, i.e., $\langle i|U_k|f\rangle$, where U_k is the rotation operator of the kth bath spin (Ref. 7, Appendix A.2). Clearly, κ depends only on the direction of the hyperfine fields and not on the time scale of the electron spin flip. The nuclei in $Mn^{(1)}$ sites do not contribute to κ since the $\mathbf{B}_{\mathrm{hyp}}$ before and after the flip are exactly antiparallel, i.e., $\omega^{\perp}(Mn^{(1)})=0$. Conversely, ^{1}H nuclei in the ligands may give a large contribution because they are subject to the vector sum of the dipolar fields from several molecules, which does not entirely reverse direction when just one molecule flips.

The other possibility is that the nuclear spins follow adiabatically the rotation of $\mathbf{S}$. For this to happen, the "bounce frequency" of $\mathbf{S}$, Ω_0, has to be small or comparable with the nuclear Larmor frequencies. Ω_0 is given here by the energy difference between the $|m|=S$ and $|m|=S-1$ cluster spin states: Since we are interested in FRMs, knowing that the resonance between $m=-S$ and $m=S-1$ states occurs at $B_z \simeq 0.39$ T (Ref. 45) yields $\hbar\Omega_0 \simeq 10$ K, i.e., several orders of magnitude larger than $\{\omega_k\}$. Therefore, the nuclei cannot adiabatically follow the dynamics of $\mathbf{S}$, and the number of spins coflipped by this mechanism, λ, is essentially zero. As a matter of nomenclature, this mechanism leads to what is called "topological decoherence" because the topological phase of the $\{\mathbf{I}_k\}$ becomes entangled with that of $\mathbf{S}$.[5–7]

Combining the two flipping mechanisms defines a parameter $\xi_0 \propto \lambda + \kappa$, which expresses how much the nuclear polarizations before and after the electron spin flip may differ for the flip to be likely to occur. Two opposite situations are sketched in Fig. 17, where we call $\mathcal{P}^{(1)}$ and $\mathcal{P}^{(2)}$ the nuclear polarizations before and after the electron spin flip, respectively. In any case, the system has to tunnel between states at the exact resonance, but in case (a) the electron flip does not require any nuclear coflip ($\mathcal{P}^{(1)}=\mathcal{P}^{(2)}$), while case (b) requires *all* nuclei to coflip ($\mathcal{P}^{(1)}=-\mathcal{P}^{(2)}$), which is extremely unlikely. As a result, the expression for the tunneling rate contains a factor $\exp(-\xi/\xi_0)$ that describes precisely this restriction. From the above discussion, it is clear that—at least in the absence of external transverse fields[76]—the main contribution to ξ_0 comes from ^{1}H nuclei, and that $\xi_0 \ll \{E_0, E_D\}$.

In the presence of a dipolar bias, the tunneling transition with the highest probability, i.e., no coflipping nuclei, occurs when $\xi_D=\xi_N$ (Fig. 16). This means that a tunneling event effectively entails an exchange of dipolar and hyperfine energy. We may then distinguish between transitions that increase the hyperfine energy ("left to right" in Fig. 16), occurring at a rate $w_\uparrow$, and transitions that decrease it ("right to left" in Fig. 16) at a rate $w_\downarrow$. The total tunneling rate is $\Gamma^N = (w_\uparrow + w_\downarrow)/2$. The PS expressions for Γ^N, generalized to the mth electronic doublet, given a (dipolar) longitudinal bias ξ on the ground doublet, are[70]

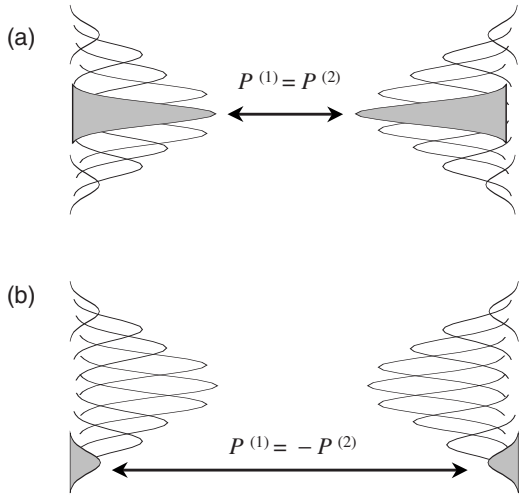

FIG. 17. Sketch of two resonant tunneling processes, differing in the number of required nuclear coflips. (a) The nuclear polarization is the same before and after the electron spin flip: This process has maximum likelihood. (b) All nuclei need to reverse their spin to conserve the total energy: This process is extremely unlikely.

$$\Gamma_m^N(\xi) \simeq \frac{2\Delta_m^2 G_N^{(m)}}{\sqrt{\pi}\hbar E_0^{(m)}} \exp(-|\xi^{(m)}|/\xi_0),$$

$$G_N^{(m)} = \exp[-\Delta_m^2/2(E_0^{(m)})^2]$$

$$E_0^{(m)} \simeq \sqrt{E_0^2 \frac{m^2}{S^2} - \Delta_m^2},$$

$$\xi^{(m)} = \xi \frac{m}{S}, \tag{10}$$

where Δ_m is the tunneling matrix element of the mth electron spin doublet, to be calculated by exact diagonalization of the giant spin Hamiltonian. The factor $G_N^{(m)}$ expresses the fact that the spin-bath-mediated tunneling rate vanishes when $\Delta_m \gg E_0^{(m)}$, i.e., when the spread of nuclear energies is not sufficient to sweep the hyperfine bias through the tunneling resonance. The parameters $E_0^{(m)}$ and $\xi^{(m)}$ are generalizations to arbitrary electron spin doublets of the quantities E_0 and ξ defined before for the ground doublet $|m|=S$, while ξ_0 is assumed m independent. To obtain the total tunneling rate through the mth doublet, we average Eq. (10) over the distribution of dipolar biases,

$$P_m(\xi) = \frac{1}{\sqrt{2\pi}E_D^{(m)}} \exp(-\xi^2/2E_D^{(m)}). \tag{11}$$

In the real situation considered here, the spread of dipolar biases in the sample is much larger than the tunneling window allowed by hyperfine couplings, $E_D \gg \xi_0$. This means that we can estimate Γ_m^N by calculating the fraction x_m^N of molecules with bias $-\xi_0^{(m)} < \xi < \xi_0^{(m)}$, for which we may approximate $\Gamma_m^N(\xi) \simeq \Gamma_m^N(0)$, and by neglecting the contribution of the molecules whose bias is larger than ξ_0 and which tunnel at an exponentially small rate,

$$\int_{-\infty}^{+\infty} P_m(\xi)\Gamma_m^N(\xi)d\xi \simeq x_m^N\Gamma_m^N(0), \tag{12}$$

$$x_m^N = \int_{-\xi_0}^{+\xi_0} P_m(\xi)d\xi. \tag{13}$$

Finally, the global spin-bath-driven tunneling rate Γ^N is obtained by summing over the m electronic doublets weighed with the appropriate Boltzmann occupation factor,

$$\Gamma^N(T) \simeq \frac{1}{Z}\sum_m \exp\left(-\frac{E_m}{k_BT}\right)x_m^N\frac{2\Delta_m^2 G_N^{(m)}}{\sqrt{\pi}\hbar E_0^{(m)}}, \tag{14}$$

where $\{E_m\}$ are the average energies of the mth doublets and Z is the partition function. Notice that the spin-bath-driven tunneling rates are individually T independent: The temperature enters only in the Boltzmann factors for the occupation of the mth doublets and, thereby, in their contribution to the global tunneling rate $\Gamma^N(T)$. Also, since $P_m(\xi)$ is essentially constant in the interval $-\xi_0<\xi<\xi_0$, we have $\Gamma_m^N \propto x_m^N \propto \xi_0$. This immediately explains why the isotopic substitution of ^{2}H for ^{1}H yields a decrease in tunneling rate [Fig. 9(a)] since these are the nuclei that mostly contribute to ξ_0.

B. Phonon-induced tunneling rate

For comparison, we also discuss the case where the electron spin tunneling is caused by spin-phonon couplings. The phonon-driven tunneling rate though the mth doublet, Γ_m^ϕ, is related to the (T-dependent) broadening of the electron spin states, $w_m(T)$, by[70,71]

$$\Gamma_m^\phi(\xi) \simeq \frac{\Delta_m^2 w_m(T)}{\xi_m^2 + \Delta_m^2 + \hbar^2 w_m^2(T)}. \tag{15}$$

The phonon-induced broadenings are obtained as a function of the sample density ρ, the sound velocity c_s, and the uniaxial anisotropy parameter D,[42]

$$w_m(T) = p_{m+1,m} + p_{m-1,m} + p_{m+2,m} + p_{m-2,m}, \tag{16a}$$

$$p_{m\pm1,m} = s_{\pm1}\frac{D^2}{12\pi\rho c_s^5\hbar^4}\frac{(E_{m\pm1}-E_m)^3}{e^{(E_{m\pm1}-E_m)/k_BT}-1}, \tag{16b}$$

$$p_{m\pm2,m} = s_{\pm2}\frac{17D^2}{192\pi\rho c_s^5\hbar^4}\frac{(E_{m\pm2}-E_m)^3}{e^{(E_{m\pm2}-E_m)/k_BT}-1}, \tag{16c}$$

with $s_{\pm1}=(S\mp m)(S\pm m+1)(2m\pm1)^2$ and $s_{\pm2}=(S\mp m)(S\pm m+1)(S\mp m-1)(S\pm m+2)$.

Again, we calculate the fraction of molecules with the highest tunneling rate, x_m^ϕ, as those whose bias is within the width of the Lorentzian function [Eq. (15)],

$$x_m^\phi = \int_{-\sqrt{\Delta_m^2+\hbar^2w_m^2(T)}}^{+\sqrt{\Delta_m^2+\hbar^2w_m^2(T)}} P_m(\xi)d\xi, \tag{17}$$

and weigh the contribution of the mth levels with their Boltzmann factor to obtain the total phonon-driven tunneling rate,

$$\Gamma^\phi(T) \simeq \frac{1}{Z}\sum_m \exp\left(-\frac{E_m}{k_BT}\right)x_m^\phi\frac{\Delta_m^2 w_m(T)}{\Delta_m^2+\hbar^2w_m^2(T)}. \tag{18}$$

Contrary to the nuclear-driven case, here, each individual mth doublet tunneling rate Γ_m^ϕ is T dependent by itself, besides being weighed by Boltzmann factors. This means that the phonon-driven tunneling rate never shows a T-independent plateau, even at very low T when tunneling occurs only through the ground doublet.

C. Tunneling rate: Longitudinal spin relaxation rate

To relate the electron spin tunneling rates $\Gamma^{N,\phi}(T)$ to the observed LSR rate W, we apply the remarks made above on the behavior of the nuclear spins upon a sudden change of the electron spin direction. In particular, we shall compare theory and experiments for the $Mn^{(1)}$ site, where (ideally) the hyperfine coupling would be strictly scalar.[50] This implies that the ^{55}Mn spin at $Mn^{(1)}$ sites do not coflip by precessional decoherence since $\omega_k^\perp \simeq 0$; neither do they coflip by topological decoherence due to the very small values of $\omega_k^\parallel/\Omega_0$. Thus, each electron spin tunneling event corresponds to the inversion of the populations of the *local* nuclear Zeeman levels. The LSR rate arising from this situation is easily obtained and can be found in the literature,[26,48,64,73] but we repeat here the derivation because it will allow us to point out exactly why no known theory can explain our data. The answer is most easily obtained for nuclear spins $I=1/2$, but remains valid for arbitrary spin values.

We start by writing a master equation for the populations of the nuclear Zeeman levels *relative to the local hyperfine field direction*, calling N_+ the number of nuclei in the excited Zeeman state and N_- those in the ground state. For simplicity, since the internal equilibrium is reestablished within a time $T_2 \ll \tau_T$ after each tunneling event, we assume that just before tunneling, all clusters have the same values of N_+ and N_-, neglecting fluctuations around the mean values. If a fast-relaxing molecule tunnels at time t, the polarization of its own nuclei is abruptly inverted. Each time a tunneling transition lowers the energy of the local nuclei, which occurs at a rate $w_\downarrow$, then N_- nuclei have been added to the total number of nuclei in the Zeeman ground state. After a time T_2, this decrease in local hyperfine bias has been redistributed over the sample, calling x_{FRM} the fraction of FRMs over the total; then, the tunneling event has increased N_+ to $N_+ + x_{FRM}N_-$. The same reasoning holds for transitions that increase the hyperfine bias. The master equation is therefore

$$\frac{dN_+}{dt} = x_{FRM}N_-w_\downarrow - x_{FRM}N_+w_\uparrow. \tag{19}$$

From here the LSR rate can be obtained by standard textbook calculations.[74] Writing $N_+=(N+n)/2$ and $N_-=(N-n)/2$, Eq. (19) becomes

$$\frac{dn}{dt} = x_{FRM}N(w_\downarrow - w_\uparrow) - x_{FRM}n(w_\downarrow + w_\uparrow), \tag{20}$$

which can be rewritten as

TABLE II. Parameter values for the calculations shown in Fig. 18. In bold are given the free fitting parameters. The tunneling matrix element in the lowest doublet, Δ_S, is obtained from the Hamiltonian [Eq. (24)], i.e., is not introduced by hand.

Panel	S	D (K)	E (K)	ξ_0 (mK)	Δ_S (μK)
(a)	10	0.524	**0.204**	**10**	5.4
(b)	10	0.524	0.204		5.4
(c)	9	0.524	**0.178**	**10**	5.6
(d)	9	0.524	0.178		5.6

$$\frac{dn}{dt} = 2W(n_0 - n), \tag{21}$$

$$n_0 = N\frac{w_\downarrow - w_\uparrow}{w_\downarrow + w_\uparrow}, \tag{22}$$

$$W = x_{\mathrm{FRM}}\frac{w_\downarrow + w_\uparrow}{2} = x_{\mathrm{FRM}}\Gamma^{N,\phi}, \tag{23}$$

where n_0 is the equilibrium nuclear polarization and W is the desired LSR rate since the solution of Eq. (21) is precisely of the form $n(t)=n(0)-[n(0)-n_0][1-\exp(-2Wt)]$.

We now attempt to fit the measured LSR rate in zero field at the $\mathrm{Mn}^{(1)}$ site in the ZFC sample, using Eqs. (14), (15), and (23). To this end, we calculate the energy level scheme of the FRMs using the effective spin Hamiltonian

$$\mathcal{H}_{\mathrm{FRM}} = -DS_z^2 + E(S_x^2 - S_y^2) - C(S_+^4 + S_-^4). \tag{24}$$

Unfortunately, very little is known about the parameter values in Eq. (24). To the best of our knowledge, it is not even established whether FRMs in Mn_{12}-ac have lowest total spin state $S=10$ or, for instance, $S=9$. The analysis of a Mn_{12} variant containing only FRMs[77] seemed to support an $S=10$ ground state, but it is not clear to what extent the FRMs in Mn_{12}-ac have the same properties as those analyzed in Ref. 77. For instance, Ref. 77 finds the first level crossing transition, i.e., the value of longitudinal field at which $E_S = E_{-S+1}$, at $B_z^{S,-S+1} \simeq 0.27$ T, quite different from the value observed for the actual FRMs in Mn_{12}-ac, $B_z^{S,-S+1} \simeq 0.39$ T.[45] We shall try both $S=10$ and $S=9$ and discuss how the different behaviors compare to the experimental data. To avoid having too many fitting parameters, we choose to keep C fixed at the value commonly used for the majority species of Mn_{12}-ac, $C=4.4\times10^{-5}$ K.[33] The uniaxial anisotropy D is obtained by imposing the condition $B_z^{S,-S+1} \simeq 0.39$ T,[45] yielding $D=g\mu_B\times0.39=0.524$ K. Although we tried adding also a fourth order term, $-BS_z^4$, it turned out that the best fits are obtained by leaving $B=0$, so we shall not discuss this further. The rhombic anisotropy term E is used as the actual fitting parameter since it most directly influences the value of the tunneling splittings $2\Delta_m$ and, thereby, the tunneling rates $\Gamma^{N,\phi}$. Carretta *et al.*[78] showed that the effective Δ is extremely sensitive to the gap between the lowest lying total spin manifolds ("S mixing") and could explain why the observed Landau-Zener tunneling probabilities in Fe_8 are much larger than what would be expected on the basis of the spin Hamiltonian parameters for the $S=10$ manifold.[79] A small gap between lowest lying total spin manifolds is quite expectable for FRMs, so the values of E that we need to justify the $\Gamma^{N,\phi}$ extracted from experiment should not be taken literally as an estimate of the anisotropy parameter. In other words, the values of E used in our calculations account also for the possible S mixing due to an energetically close manifold with different total spins S, and do not necessarily correspond to the values that one would obtain from neutrons scattering or EPR experiments. We take as fixed parameters the sound velocity $c_s=1.5\times10^3$ m/s (Ref. 80), the density $\rho=1.83\times10^3$ g/m^3 (Ref. 31), $E_D=0.32$ K (Ref. 63), and $E_0=0.082$ K (Ref. 70), whereas ξ_0 is allowed to vary. When comparing nuclear- and phonon-driven tunneling rates, we impose the same parameters for the spin Hamiltonian [Eq. (24)]. The results of the calculations are shown in Fig. 18, for the set of parameters given in Table II.

By looking at the theoretical curves alone, we find that, given a fixed set of parameters for the FRMs' spin Hamiltonian [Eq. (24)], the nuclear-driven tunneling process always dominates over the phonon-driven one, both in the low-T and in the high-T regime. The situation may be reversed in the high-T regime by assuming that the sound velocity is lower than the literature value used here, but $\Gamma^\phi > \Gamma^N$ would never hold at low T under realistic circumstances. A comparison with the experimental data shows that both nuclear- and phonon-driven mechanisms yield a correct slope of $W(T)$ in the thermally assisted regime, $T>0.8$ K, whereas the phonon process can never reproduce the low-T plateau. An almost perfect fit of the data is obtained by assuming that the FRMs have a total spin $S=9$, while the $S=10$ case has a T-dependent region systematically starting at too high temperatures. In the nuclear-driven case, we used an optimal value of $\xi_0 \simeq 10$ mK, which seems very reasonable, since the main contribution to ξ_0 arises from the coupling to protons. Conversely, the values used for E appear very high since to fit the NMR data we need to assume $D/E \simeq 2.5$. As mentioned before, however, such a high value of E should not be interpreted as the spectroscopic rhombic term in the spin Hamiltonian since it is used here as the parameter that tunes the tunneling splitting of the ground doublet and, therefore, incorporates the effect of S mixing[78] if a manifold with different total spin values is energetically close to the S ground state.

An important remark is that our calculations, which only account for tunneling fluctuations as a source of nuclear

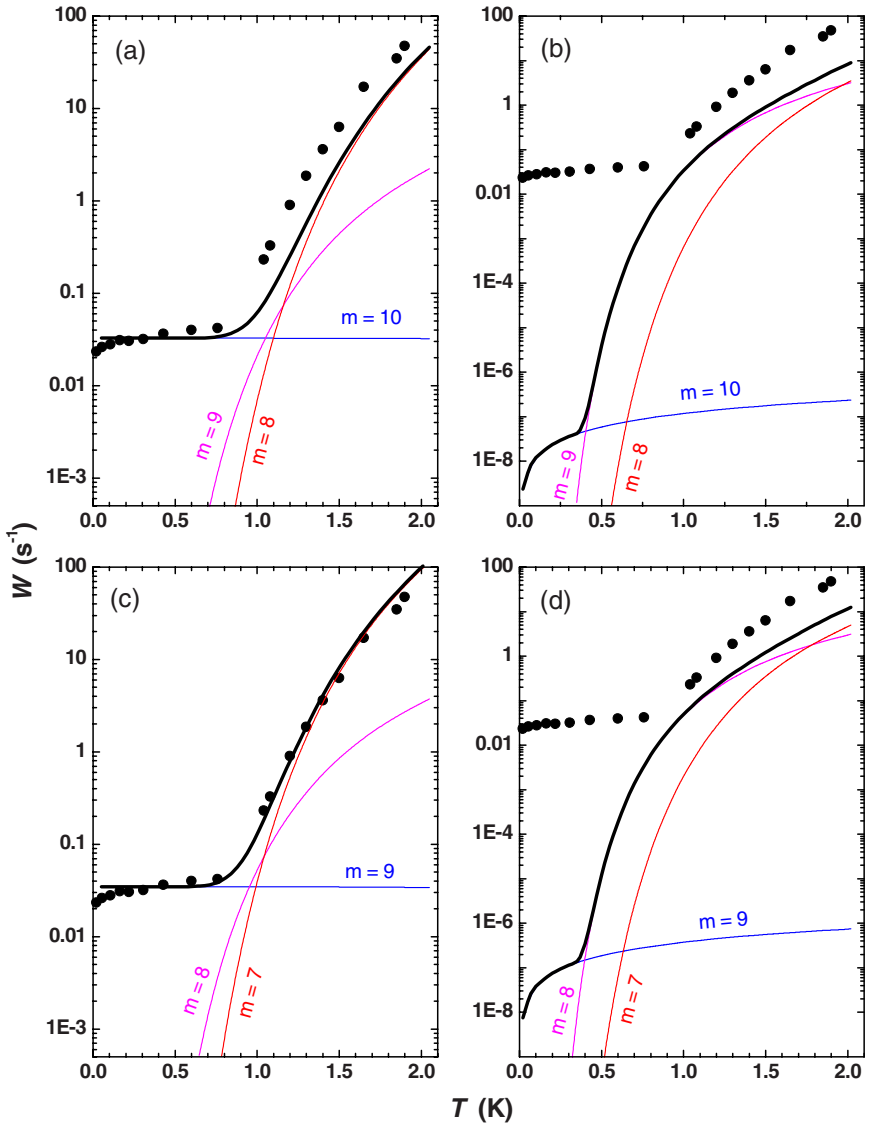

FIG. 18. (Color online) Calculated nuclear spin-lattice relaxation rates W as a function of temperature for spin-bath [panels (a) and (c)] and phonon [panels (b) and (d)] mediated tunneling. In panels (a) and (b), a total spin $S=10$ is assumed for the FRMs; in panels (c) and (d), $S=9$. The complete parameter sets are given in Table II. Black dots: experimental data; thick black lines: calculated W; thin lines: contributions of the mth electron spin doublets to the total rate.

LSR, can accurately reproduce the observed LSR rate *also in the thermally activated regime*, $T>0.8$ K. All the previous NMR experiments in that regime[24,27,49,81] have been interpreted in terms of the intrawell electron spin fluctuations, which arise from thermal excitation of the electron spin state on the same side of the anisotropy barrier [see Fig. 1(b)]. As pointed out by Goto *et al.*,[24] that reasoning is inappropriate when applied to the LSR of nuclei belonging to Mn^{4+} ions since the hyperfine coupling tensor is diagonal. In that case, a fluctuation in the $\hat{z}$ projection of the electron spin does not result in a fluctuating field perpendicular to the nuclear quantization axis (which is $\hat{z}$ itself) and cannot account for longitudinal nuclear spin relaxation. As we show in Fig. 18, including the effect of electron spin tunneling through $|m|<S$ doublets solves what appeared to be a paradox since the tunneling fluctuations induce nuclear LSR also in the absence of nondiagonal hyperfine coupling terms. For the nuclei in Mn^{3+} ions, the intrawell electron spin transitions do provide an additional channel for nuclear relaxation, which may explain why the LSR rate at $T>1$ K in the Mn^{3+} sites is larger than that in the Mn^{4+} ones.[24,49]

D. Thermal equilibrium

In the preceding discussion, it may seem that we have not explicitly used the condition that the nuclear spins are in thermal equilibrium, which is what we observe in the experiment. This condition, however, is automatically implied in the application of Eq. (23) to the LSR rate. For Eq. (23) to actually represent the rate at which the nuclear spins exchange energy with a thermal bath and thereby return to the equilibrium magnetization after a perturbing NMR pulse, one needs to include the detailed balance condition,

$$\frac{w_{\uparrow}}{w_{\downarrow}} = \exp\left(-\frac{\hbar\omega_N}{k_B T}\right). \quad (25)$$

In other words, if the nuclear spin temperature has to reach equilibrium with the thermal (phonon) bath via the process described by the rates $w_{\uparrow}$ and $w_{\downarrow}$, the latter *must* satisfy Eq. (25). The detailed balance condition is often taken for granted, but in this case one needs to be more careful. $w_{\uparrow}$ and $w_{\downarrow}$ represent the rates of *electron spin transitions* that increase or lower the nuclear energy, respectively. The crucial point is that both are rates for *tunneling* transitions, which occur when the *total energy* of the "electron plus nuclear spin" system is the same before and after the electron spin flip. Thus, the difference between $w_{\uparrow}$ and $w_{\downarrow}$ is simply that, $w_{\uparrow}$ is the rate for a tunneling transition that increases the nuclear spin energy while reducing the electronic one. That is, after the flip, most of the nuclei are oriented against their local hyperfine field, while the electron spin is favorably aligned with respect to the local field (in particular the dipolar one, when $B_z=0$). $w_{\downarrow}$ does the opposite and, interestingly, this means that the instantaneous local spin temperature (local referring to the nuclei belonging to a specific molecule that has just flipped) is negative. This situation is clearly very different from the standard NMR picture of nuclear relaxation by coupling to paramagnetic centers, where the latter make spin-phonon transitions between Zeeman-split levels having different thermal populations.

Now, we can summarize the meaning of our experimental results for the description of electron spin tunneling in the presence of a nuclear spin bath.

(i) The Prokof'ev-Stamp theory of the spin bath, as developed so far and reviewed in Sec. V A, quantitatively and qualitatively reproduces the nuclear LSR rate in the whole temperature regime of our measurements by assuming that the LSR is due to tunneling events in a minority of fast-tunneling molecules.

(ii) The additional observation that the nuclear spins are in thermal equilibrium with the phonon lattice at all temperatures implies that *the rates* $w_{\uparrow}$ *and* $w_{\downarrow}$ *must be different*. For this to happen, it is necessary to explicitly include the role of spin-phonon interactions in the nuclear-spin mediated tunneling process. Importantly, the results of the calculations shown in Figs. 18(b) and 18(d) indicate that it is not sufficient to attribute the thermal relaxation to a phonon-assisted tunneling process, as described in Sec. V B working "in parallel" to the nuclear-spin-mediated tunneling process. At the lowest temperatures, even the longest thermalization times observed in our experiments (Sec. IV A) are still much shorter than $(\Gamma^{\phi})^{-1}$, as calculated from phonon-assisted tunneling alone (Sec. V B), thus reinforcing the need for a theory that includes nuclear-spin and phonon mediated tunneling *at the same time*.

(iii) Our statement that the nuclear relaxation has to be mediated by inelastic electron spin tunneling processes is further supported by specific heat experiments that show that a system of dipolarly coupled tunneling molecules can relax to the long-range ferromagnetically ordered state, provided that the tunneling rate is fast enough for the experimental detection of the ordering anomaly.[72] This means that *there is a mechanism for the ensemble of electron spins to find its thermodynamic ground state*, even at temperatures so low that the relaxation can only proceed by quantum tunneling. *We argue here that such inelastic tunneling mechanism is the same mechaninsm that is responsible for the thermalization of the nuclear spins.* Indeed, by extending the specific heat measurements below the ordering temperature, one even observes the equilibrium specific heat contribution of the nuclear spins, meaning that both the electron spins and the nuclear spins can attain thermal equilibrium within the time scale of the specific heat experiment (10–100 s) at all temperatures reached.

All the work presented here is dedicated to the small-Δ_0 incoherent tunneling regime for the central spin. Having shown that the description of the nuclear-spin-mediated tunneling is incomplete without the inclusion of spin-phonon couplings, some concerns may be raised also on the current description of the spin-bath effects on the electron spin in the large-Δ_0 coherent tunneling regime.[82,83] This work cannot address that issue, and we think that the answer will have to come from low-T NMR experiments in a large transverse field and a *quantitative* analysis of pulsed-ESR experiments.

VI. CONCLUDING REMARKS

The purpose of the research presented here is to illustrate and analyze a prototypical example of quantum tunneling of a macroscopic variable (the giant spin of a single-molecule magnet) in the presence of a spin-bath environment. Instead of looking at the macroscopic variable itself and deducing the effect of the environment on its dynamics, as is most often done, we have directly observed the behavior of the spin bath by means of low-T NMR experiments.

We have provided compelling evidence that the longitudinal nuclear spin relaxation in the ^{55}Mn nuclei of Mn_{12}-ac is driven by electron-spin quantum tunneling fluctuations. The nuclear LSR rate W indeed contains all the features that are expected to be associated with tunneling of the molecular spin: (i) a T-independent plateau of the LSR rate for $T < 0.8$ K, (ii) a strong dependence of W on a longitudinal magnetic field, which destroys the resonance condition for electron spin tunneling, (iii) the slowing down of the nuclear LSR upon isotropic substitution of ^{1}H by ^{2}H in the ligands by an amount identical to the slowing down of the quantum relaxation of the magnetization observed in similar systems. Because of the short time scale of the observed LSR, we argued that the tunneling fluctuations must take place in a minority of fast-relaxing molecules, which are indeed known to be present in Mn_{12}-ac. For these fluctuations to relax the nuclear magnetization in the entire sample, an additional mechanism is required, which equilibrates the nuclear spin polarization across neighboring molecules, i.e., intercluster nuclear spin diffusion. Our data on the transverse nuclear spin relaxation show that the intercluster spin diffusion is indeed present and effective. All the above observations confirm and support the picture of nuclear-driven quantum tunneling of magnetization as originally formulated by Prokof'ev and Stamp. However, a crucial outcome of our experiments is the demonstration that the nuclear spins are in

thermal equilibrium with the lattice phonons down to the lowest temperatures, where only quantum tunneling fluctuations of the electron spins are still present. This observation cannot be explained within the present theory of the spin bath.

The implications of our results are potentially very profound, particularly because of the growing interest toward a coherent manipulation of spins for quantum information processing. The spin-bath environment, describing localized two-level systems, has been repeatedly identified as the most important source of decoherence in solid-state qubits. This includes superconducting systems,[84] quantum dots,[85,86] nitrogen-vacancy centers in diamond,[87] and, of course, molecular magnets.[20] We have investigated here the incoherent tunneling regime, but the theoretical formalism to describe the coupling between central spin and spin bath is identical in the case of coherent spin dynamics. Therefore, the main finding of our work–that the role of phonons in the nuclear-spin mediated tunneling is currently lacking a proper description–suggests that also the contribution of the nuclear spin bath to the decoherence rate of realistic spin qubits may need to be revisited.

ACKNOWLEDGMENTS

We are indebted to O. N. Bakharev, H. B. Brom, D. Bono, N. J. Zelders, and G. Frossati for experimental help and extensive discussions. Continuous and illuminating theoretical support from P. C. E. Stamp and I. S. Tupitsyn is gratefully acknowledged, and so are discussions with W. Wernsdorfer, S. Hill, N. V. Prokof'ev, B. V. Fine, M. Evangelisti, A. J. Leggett, Y. Imry, M. Schechter, and A. L. Burin. We also thank K. Awaga and K. Takeda for useful correspondence about their results in Ref. 77. The Mn_{12}-ac samples were supplied by R. Sessoli and A. Caneschi (crystallites, natural and deuterated) and A. Millan (single crystal). This work is part of the research program of the "Stichting FOM" and is partially funded by the EC-RTN "QuEMolNa" and EC-Network of Excellence "MAGMANet" (No. 515767-2).

*a.morello@unsw.edu.au

[1] Y. Nakamura, Yu. A. Paskin, and J. S. Tsai, Nature (London) **398**, 786 (1999).
[2] D. Vion, A. Aassime, A. Cottet, P. Joyez, H. Pothier, C. Urbina, D. Esteve, and M. H. Devoret, Science **296**, 886 (2002).
[3] I. Chiorescu, Y. Nakamura, C. J. P. M. Harmans, and J. E. Mooij, Science **299**, 1863 (2003).
[4] A. J. Leggett, S. Chakravarty, A. T. Dorsey, M. P. A. Fisher, A. Garg, and W. Zwerger, Rev. Mod. Phys. **59**, 1 (1987).
[5] N. V. Prokof'ev and P. C. E. Stamp, arXiv:cond-mat/9511011 (unpublished).
[6] N. V. Prokof'ev and P. C. E. Stamp, J. Low Temp. Phys. **104**, 143 (1996).
[7] N. V. Prokof'ev and P. C. E. Stamp, Rep. Prog. Phys. **63**, 669 (2000).
[8] D. Gatteschi, A. Caneschi, L. Pardi, and R. Sessoli, Science **265**, 1054 (1994).
[9] G. Christou, D. Gatteschi, D. N. Hendrickson, and R. Sessoli, MRS Bull. **25**, 66 (2000).
[10] D. Gatteschi and R. Sessoli, Angew. Chem., Int. Ed. **42**, 268 (2003).
[11] E. M. Chudnovsky and L. Gunther, Phys. Rev. Lett. **60**, 661 (1988).
[12] L. Thomas, F. Lionti, R. Ballou, D. Gatteschi, R. Sessoli, and B. Barbara, Nature (London) **383**, 145 (1996).
[13] J. R. Friedman, M. P. Sarachik, J. Tejada, and R. Ziolo, Phys. Rev. Lett. **76**, 3830 (1996).
[14] J. M. Hernández, X. X. Zhang, F. Luis, J. Bartolomé, J. Tejada, and R. Ziolo, Europhys. Lett. **35**, 301 (1996).
[15] C. Sangregorio, T. Ohm, C. Paulsen, R. Sessoli, and D. Gatteschi, Phys. Rev. Lett. **78**, 4645 (1997).
[16] N. V. Prokof'ev and P. C. E. Stamp, Phys. Rev. Lett. **80**, 5794 (1998).
[17] W. Wernsdorfer, T. Ohm, C. Sangregorio, R. Sessoli, D. Mailly, and C. Paulsen, Phys. Rev. Lett. **82**, 3903 (1999).
[18] W. Wernsdorfer, A. Caneschi, R. Sessoli, D. Gatteschi, A. Cornia, V. Villar, and C. Paulsen, Phys. Rev. Lett. **84**, 2965 (2000).
[19] M. Evangelisti, F. Luis, F. L. Mettes, R. Sessoli, and L. J. de Jongh, Phys. Rev. Lett. **95**, 227206 (2005).
[20] A. Ardavan, O. Rival, J. J. L. Morton, S. J. Blundell, A. M. Tyryshkin, G. A. Timco, and R. E. P. Winpenny, Phys. Rev. Lett. **98**, 057201 (2007).
[21] A. Keren, O. Shafir, E. Shimshoni, V. Marvaud, A. Bachschmidt, and J. Long, Phys. Rev. Lett. **98**, 257204 (2007).
[22] J. Villain, Eur. Phys. J. B **48**, 173 (2005).
[23] A. Morello, O. N. Bakharev, H. B. Brom, R. Sessoli, and L. J. de Jongh, Phys. Rev. Lett. **93**, 197202 (2004).
[24] T. Goto, T. Koshiba, T. Kubo, and K. Agawa, Phys. Rev. B **67**, 104408 (2003).
[25] M. Ueda, S. Maegawa, and S. Kitagawa, Phys. Rev. B **66**, 073309 (2002).
[26] S. H. Baek, F. Borsa, Y. Furukawa, Y. Hatanaka, S. Kawakami, K. Kumagai, B. J. Suh, and A. Cornia, Phys. Rev. B **71**, 214436 (2005).
[27] N. E. Chakov, S.-C. Lee, A. G. Harter, P. L. Kuhns, A. P. Reyes, S. O. Hill, N. S. Dalal, W. Wernsdorfer, K. A. Abboud, and G. Christou, J. Am. Chem. Soc. **128**, 6975 (2006).
[28] A. J. Leggett, Suppl. Prog. Theor. Phys. **69**, 80 (1980).
[29] A. J. Leggett, J. Phys.: Condens. Matter **14**, R415 (2002).
[30] M. Arndt, A. Nairz, J. Vos-Andreae, C. Keller, G. van der Zouw, and A. Zeilinger, Nature (London) **401**, 680 (1999).
[31] T. Lis, Acta Crystallogr., Sect. B: Struct. Crystallogr. Cryst. Chem. **B36**, 2042 (1980).
[32] R. Sessoli, H.-L. Tsai, A. R. Schake, S. Wang, J. B. Vincent, K. Folting, D. Gatteschi, G. Christou, and D. N. Hendrickson, J. Am. Chem. Soc. **115**, 1804 (1993).
[33] I. Mirebeau, M. Hennion, H. Casalta, H. Andres, H. U. Güdel, A. V. Irodova, and A. Caneschi, Phys. Rev. Lett. **83**, 628 (1999).
[34] A. L. Barra, D. Gatteschi, and R. Sessoli, Phys. Rev. B **56**, 8192 (1997).

[35] S. Hill, J. A. A. J. Perenboom, N. S. Dalal, T. Hathaway, T. Stalcup, and J. S. Brooks, Phys. Rev. Lett. **80**, 2453 (1998).
[36] The anisotropy parameters obtained by EPR seem to depend on the magnetic field range used in the experiment (Refs. 34 and 35), whereas neutron scattering is a zero-field experiment and does not require assumptions on the **g** tensor in order to fit the data.
[37] S. Hill, R. S. Edwards, S. I. Jones, N. S. Dalal, and J. M. North, Phys. Rev. Lett. **90**, 217204 (2003).
[38] E. del Barco, A. D. Kent, E. M. Rumberger, D. N. Hendrickson, and G. Christou, Phys. Rev. Lett. **91**, 047203 (2003).
[39] A. Cornia, R. Sessoli, L. Sorace, D. Gatteschi, A. L. Barra, and C. Daiguebonne, Phys. Rev. Lett. **89**, 257201 (2002).
[40] A. G. Harter, N. E. Chakov, B. Roberts, R. Achey, A. Reyes, P. Kuhns, G. Christou, and N. S. Dalal, Inorg. Chem. **44**, 2122 (2005).
[41] F. Hartmann-Boutron, P. Politi, and J. Villain, Int. J. Mod. Phys. B **10**, 2577 (1996).
[42] M. N. Leuenberger and D. Loss, Phys. Rev. B **61**, 1286 (2000).
[43] S. M. J. Aubin, Z. Sun, I. A. Guzei, A. L. Rheingold, G. Christou, and D. N. Hendrickson, Chem. Commun. (Cambridge) **1997**, 2239.
[44] M. Evangelisti, J. Bartolomé, and F. Luis, Solid State Commun. **112**, 687 (1999).
[45] W. Wernsdordfer, R. Sessoli, and D. Gatteschi, Europhys. Lett. **47**, 254 (1999).
[46] Z. Sun, D. Ruiz, N. R. Dilley, M. Soler, J. Ribas, K. Folting, M. B. Maple, G. Christou, and D. N. Hendrickson, Chem. Commun. (Cambridge) **1999**, 1973.
[47] W. Wernsdordfer (unpublished).
[48] A. Morello, Ph.D. thesis, Leiden University, arXiv:cond-mat/0404049.
[49] Y. Furukawa, K. Watanabe, K. Kumagai, F. Borsa, and D. Gatteschi, Phys. Rev. B **64**, 104401 (2001).
[50] T. Kubo, T. Goto, T. Koshiba, K. Takeda, and K. Awaga, Phys. Rev. B **65**, 224425 (2002).
[51] A. Suter, M. Mali, J. Roos, and D. Brinkmann, J. Phys.: Condens. Matter **10**, 5977 (1998).
[52] A. Morello, O. N. Bakharev, H. B. Brom, and L. J. de Jongh, Polyhedron **22**, 1745 (2003).
[53] T. Kubo, T. Koshiba, T. Goto, A. Oyamada, Y. Fujii, K. Takeda, and K. Awaga, Physica B **294-295**, 310 (2001).
[54] T. Goto, T. Kubo, T. Koshiba, Y. Fujii, A. Oyamada, J. Arai, K. Takeda, and K. Awaga, Physica B **284-288**, 1227 (2000).
[55] I. Chiorescu, R. Giraud, A. G. M. Jansen, A. Caneschi, and B. Barbara, Phys. Rev. Lett. **85**, 4807 (2000).
[56] L. Bokacheva, A. D. Kent, and M. A. Walters, Phys. Rev. Lett. **85**, 4803 (2000).
[57] L. Thomas, A. Caneschi, and B. Barbara, Phys. Rev. Lett. **83**, 2398 (1999).
[58] J. H. Van Vleck, Phys. Rev. **74**, 1168 (1948).
[59] D. Bono, J. Hartig, M. Huber, H. Schnökel, and L. J. de Jongh, J. Cluster Sci. **18**, 319 (2007).
[60] M. Takigawa and G. Saito, J. Phys. Soc. Jpn. **55**, 1233 (1986).
[61] M. Soler, W. Wernsdorfer, Z. Sun, J. C. Huffman, D. N. Hendrickson, and G. Christou, Chem. Commun. (Cambridge) **2003**, 2672.
[62] W. Wernsdorfer, M. Murugesu, and G. Christou, Phys. Rev. Lett. **96**, 057208 (2006).
[63] I. S. Tupitsyn (private communication).
[64] A. Abragam, *The Principles of Nuclear Magnetism* (Oxford University Press, London, 1961).
[65] M. Goldman, *Spin Temperature and Nuclear Magnetic Resonance in Solids* (Oxford University Press, London, 1970).
[66] C. Paulsen, J.-G. Park, B. Barbara, R. Sessoli, and A. Caneschi, J. Magn. Magn. Mater. **140-144**, 1891 (1995).
[67] Y. Suzuki, M. P. Sarachik, E. M. Chudnovsky, S. McHugh, R. Gonzalez-Rubio, N. Avraham, Y. Myasoedov, E. Zeldov, H. Shtrikman, N. E. Chakov, and G. Christou, Phys. Rev. Lett. **95**, 147201 (2005).
[68] J. Tejada, E. M. Chudnovsky, J. M. Hernandez, and R. Amigó, Appl. Phys. Lett. **84**, 2373 (2004).
[69] T. Goto, T. Koshiba, A. Oyamada, T. Kubo, Y. Suzuki, K. Awaga, B. Barbara, and J.-P. Boucher, Physica B **329-333**, 1185 (2003).
[70] P. C. E. Stamp and I. S. Tupitsyn, Chem. Phys. **296**, 281 (2004).
[71] Yu. Kagan and L. A. Maksimov, Sov. Phys. JETP **52**, 688 (1980).
[72] M. Evangelisti, F. Luis, F. L. Mettes, N. Aliaga, G. Aromí, J. J. Alonso, G. Christou, and L. J. de Jongh, Phys. Rev. Lett. **93**, 117202 (2004).
[73] S. Alexander and A. Tzalmona, Phys. Rev. **138**, A845 (1965).
[74] C. P. Slichter, *Priciples of Magnetic Resonance* (Springer-Verlag, Berlin, 1990).
[75] I. J. Lowe and D. Tse, Phys. Rev. **166**, 279 (1968).
[76] I. S. Tupitsyn, P. C. E. Stamp, and N. V. Prokof'ev, Phys. Rev. B **69**, 132406 (2004).
[77] K. Takeda, K. Awaga, T. Inabe, A. Yamaguchi, H. Ishimoto, T. Tomita, H. Mitamura, T. Goto, N. Mori, and H. Nojiri, Phys. Rev. B **65**, 094424 (2002).
[78] S. Carretta, E. Liviotti, N. Magnani, P. Santini, and G. Amoretti, Phys. Rev. Lett. **92**, 207205 (2004).
[79] W. Wernsdordfer and R. Sessoli, Science **284**, 133 (1999).
[80] F. L. Mettes, F. Luis, and L. J. de Jongh, Phys. Rev. B **64**, 174411 (2001).
[81] A. Lascialfari, Z. H. Jang, F. Borsa, P. Carretta, and D. Gatteschi, Phys. Rev. Lett. **81**, 3773 (1998).
[82] P. C. E. Stamp and I. S. Tupitsyn, Phys. Rev. B **69**, 014401 (2004).
[83] A. Morello, P. C. E. Stamp, and I. S. Tupitsyn, Phys. Rev. Lett. **97**, 207206 (2006).
[84] J. M. Martinis, K. B. Cooper, R. McDermott, M. Steffen, M. Ansmann, K. D. Osborn, K. Cicak, S. Oh, D. P. Pappas, R. W. Simmonds, and C. C. Yu, Phys. Rev. Lett. **95**, 210503 (2005).
[85] F. H. L. Koppens, J. A. Folk, J. M. Elzerman, R. Hanson, L. H. Willems van Beveren, I. T. Vink, H. P. Tranitz, W. Wegscheider, L. P. Kouwenhoven, and L. M. K. Vandersypen, Science **309**, 1346 (2005).
[86] A. C. Johnson, J. R. Petta, J. M. Taylor, A. Yacoby, M. D. Lukin, C. M. Marcus, M. P. Hanson, and A. C. Gossard, Nature (London) **435**, 925 (2005).
[87] L. Childress, M. V. Gurudev Dutt, J. M. Taylor, A. S. Zibrov, F. Jelezko, J. Wrachtrup, P. R. Hemmer, and M. D. Lukin, Science **314**, 281 (2006).